UNIVERSITY OF COPENHAGEN
FACULTY OF SCIENCE

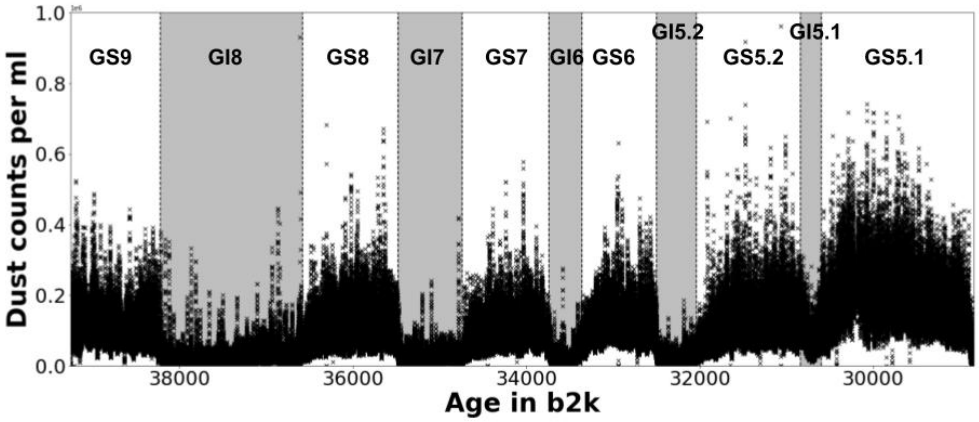

M.Sc. Thesis

The EGRIP Dustprofile

Investigating dust content of 40,000 year old Greenland ice

Marie Cecilie Boysen

Supervisors: Helle Astrid Kjær and Anders Svensson

Submitted: June 6, 2023

Abstract

One of the greatest challenges to contemporary society is global warming. Understanding future climate changes requires a detailed knowledge of its development in the past. The Greenland ice sheet offers a unique record of climate changes that occurred in the past 100 thousand years, the study of which was intensified in past years.

One interesting property of the ice is the dust content that is believed to play a major role on climate change.

Through Continuous Flow Analysis (CFA), this thesis measures the amount and size distribution of dust in ice drilled from the East Greenland Ice core Project (EGRIP). Measurements of particle size and amount are made with an Abakus laser counter. The resulting data covers stadials 9 to 5 of the Last Glacial Period 30-40.000 years ago, corresponding to a depth range of 1725-1925 meters. The thesis is a side product of the EGRIP gas measurement campaign at the Physics of Ice, Climate, and Earth (PICE) section of the Niels Bohr Institute (NBI) held in August til September 2022.

The data processing is presented and the resulting dust profile is analysed and compared to earlier CFA records of soluble dust (Ca2+) from NGRIP, GRIP and GISP2 for the same period.

The dust profile was found to have a good correlation with the Greenland stadials 5.1 to 9, with stadials having up to 8 times more dust than the interstadials. A correlation between the $\delta^{18}O$ temperature proxy and dust measurements is observed, and it is indicated that the warming in the Dansgaard-Oeschger events appeared abrupt, whereas the cooling was gradual.

The record of large fraction particles are compared to events of fires and volcanic eruptions finding only occasional matches.

Contents

1 Introduction

Greenland, one of the least dense populated areas in the world, offers the material, for the scientific research field Paleoclimatology: Greenlandic ice.

Except for just the southern tip, Greenland lies completely north of the 60 degrees north latitude. This location implies a relatively cold climate and a substantial snow fall. Layers of snow from more than 128,000 years have accumulated to form the Greenland ice sheet (in Danish 'Indlandsisen') that covers nearly 80% of Greenland and has an average thickness of about 1.5 km and over 3 km at its thickest point.

By dating and examining the ice-layers, the ice sheet reveals a scientific valuable record of past climates, e.g. by observing the content of $\delta^{18}O$, as discovered by Willi Dansgaard back in the 1950's [1, 2]. Various core drilling projects have taken place since then and ice from one of these drillings is the subject for this thesis. We shall obtain and analyse the dust enclosed in the ice and see if and how the dust profile correlates to variations of the climate in the past.

The ice core drilling of interest here is the East Greenland Ice Core Project (EGRIP). The project began in 2015 and is ongoing [3]. The location of this drilling is right on the North East Greenland Ice Stream (NEGIS). This location and those of other drillings can be seen in figure (1). The aim of the campaign is to drill an ice core more than 2550 meters deep.

In detail, this paper is concerned with obtaining, processing and interpreting the insoluble dust profile from EGRIP in an interval covering several Dansgaard-Oeschger (DO) events.

A substantial part of this work was experimental in terms of participating in the EGRIP gas measurement campaign at the section of Physics of Ice Climate and Earth (PICE) at the Niels Bohr Institute (NBI), which was held in August-September 2022. In this campaign, ice from almost 2000 m deep and up to ca. 1700 m was melted and analysed. Ice from these depths is between 29 and 39 thousand years old, counting before the year 2,000 (ka b2k). It covers the DO-events 5.1 to 9 (the original intention was to cover DO-events 2 to 8 [4] which would have required more ice than what the campaign for practical reasons could encompass).

During the campaign, the dust profile was obtained on an 'Abakus' in-

strument that measures the dust concentration as well as size fractions of individual dust particles from a continuous melt stream of the ice core. The measurements were processed into a continuous, calibrated profile, and the result compared to existing Greenland dust profiles covering the same time period.

This paper takes you through the basic concepts underlying this research starting by the geological perspective of this time period, taking you through more details about ice cores and what the dust-content implies for the climate. Further, the methods by which the results have been obtained are explained. Finally, results are discussed and analysed, followed by my conclusion.

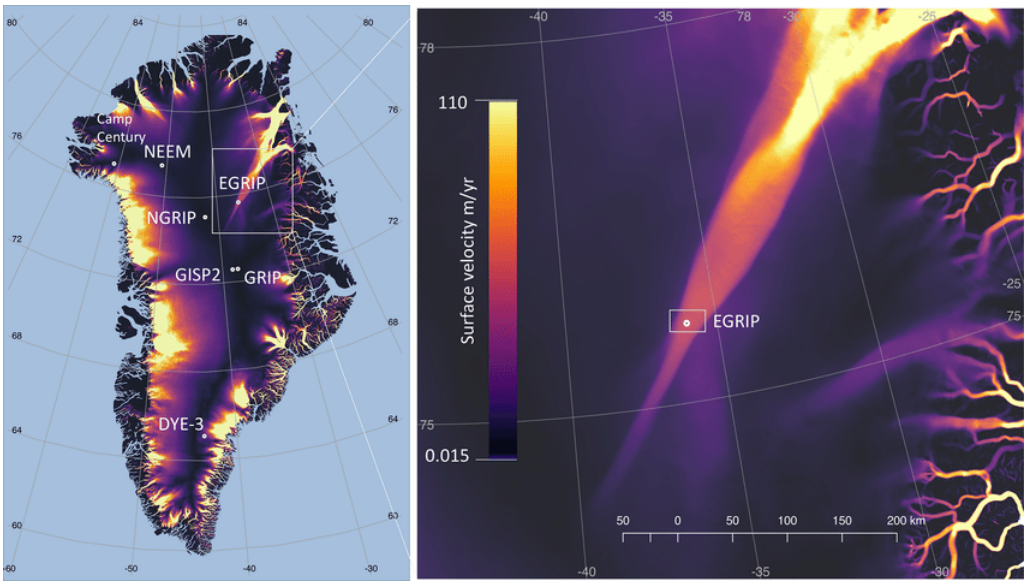

Figure 1: Positions of the different Greenland ice drilling sites. Colours show surface flow velocities [5]

2 Background

2.1 Geological Perspective and Climate Fluctuations of the Past

Climate change is one of the biggest challenges for contemporary society. However it is hardly a new phenomenon. Looking back in time, Earth has seen numerous climate fluctuations in the past; Dinosaurs roamed a subtropical Northern Europe 80 million years ago [6], whereas 50.000 years ago, in the same area, one would instead find arctic Wolly Mammoths roaming the plains of the last ice age [7]. Earths geological history is sketched in figure (3).

Global climate fluctuations of several tens of degrees may naturally happen across millions of years. These fluctuations are caused by various complicated processes like carbon dioxide concentrations in the atmosphere, tilting of Earths axis or solar cycles [8] to mention a few. In the case of the dinosaurs, tectonic plate movement also plays a role to the local climate of Northern Europe [6]. Many aspects are still uncertain and further research into ancient climate called Paleoclimatology will help understanding recent global warming.

This thesis considers climate fluctuations in a relatively short period ∼30-40.000 years b2k, - a very small part of the Pleistocene Epoch (∼10.000-2 million years b2k [9]). The Pleistocene is generally characterised by a cold climate and ice covering about a third of Earths landmass including Greenland [10]. Within the Pleistocene, a number of relatively cold and warm periods have been observed (see figure (2)). Known as glacials and interglacials, these mark long periods of advancing and retreating glacial ice with corresponding changes in sea level. Interglacials last about 10.000 years whereas glacials can last anywhere from 50.000-70.000 years [11].

Figure 2: Glacial-interglacial cycles of the past 450.000 years to the present. (Adapted from [12])

Measurements of climate in the Pleistocene is remarkably detailed. The remaining ice from this period, deposited deep within the ice sheets of Greenland, hold much information about the climate at this time. Temperature when the ice was deposited is indicated by the content of O_{18} isotopes in the ice [2]. This measurement is known as $\delta^{18}O$. Other environmental factors may be gathered from analyses of dust and gas in the ice. Further information on the relationship of dust and climate is given in section 2.6.

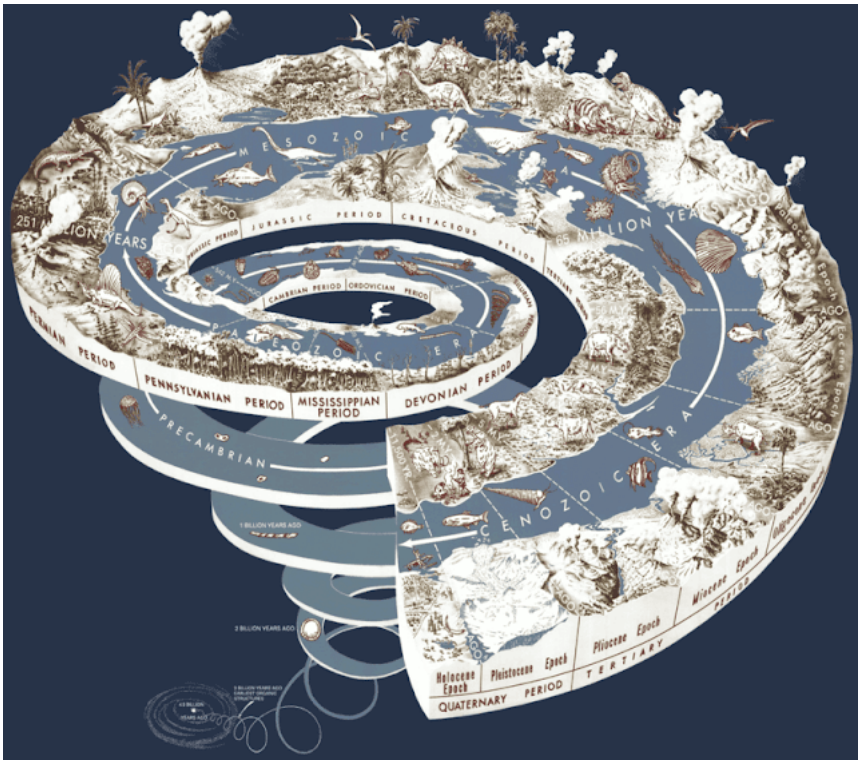

Figure 3: Illustrative representation of the history of our planet Earth. It is traditionally parted in eons, eras, epochs and periods. The Pleistocene Epoch contains the records investigated in this thesis. The Holocene epoch represents the current epoch (as of 2023). (Adapted from [13])

2.2 Last Glacial Period

Earth is currently experiencing a 10.000 year long interglacial period known as the Holocene. Before that, the Last Glacial Period (LGP) reigned. It was a time interval between 115,000 and 11,700 years b2k towards the end of the Pleistocene epoch and was characterised by a cold climate during which glaciers advanced and covered big parts of North America, Northern Europe and Russia (see figure (4)).

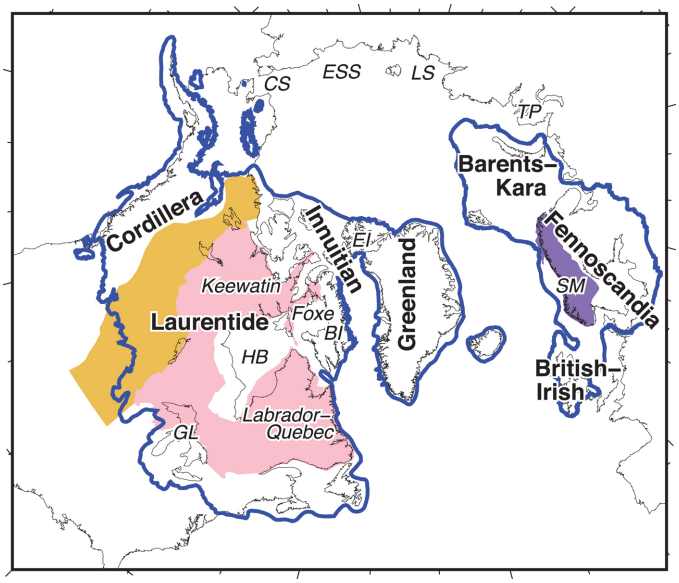

Figure 4: Locations of ice sheets in the Northern Hemisphere during the Last Glacial Maximum (21 ka b2k) marked in blue. (Adapted from [14])

2.3 Dansgaard-Oeschger Events

But even though the LGP was a cold period, there were fluctuations between colder and warmer intervals. These so-called stadials and interstadials lasted from a few hundred up to more than a thousand years [15]. The fluctuation from the cold stadial to the warm interstadial and back, first described by Willi Dansgaard and Hans Oeschger, is called a DO-event. [16, 17, 18, 19]. These are well documented climate fluctuations found in the Greenland ice cores from the LGP and speculated to also exist in other glacial periods. They are characterised by abrupt warming and gradual cooling and occurred 25 times during the LGP. The causes for the events are debated [20, 19]. Dust is regarded a possible major driver [21]. Possible other explanations could stem from changes in the intensity of the Atlantic Meridional Overturning Circulation (AMOC), which leads to heat trans- port changes from low to high latitudes. But also sea ice changes or even unknown solar cycles have been suggested as the root cause [19, 22].

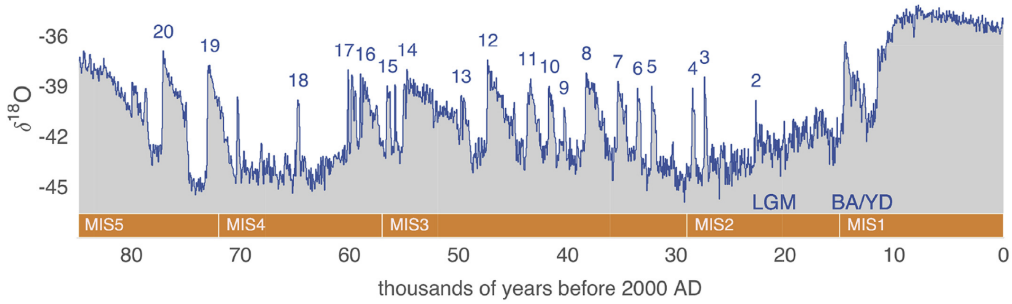

Figure 5: DO events indicated through $\delta^{18}O$ of NGRIP ice spanning a period from $\sim$ 80.000 yrs b2k to the present. The current project considers ice from the period $\sim$ 39.000 to $\sim$ 29.000 yrs b2k. DO events are indicated with blue numbers, enumerated backwards in time. (Reproduced from [19]).

2.4 Ice Cores

On the Greenland Ice Sheet snow fall accumulates in annual layers. The ice situated the deepest in the ice sheet forms thinner layers due to compression at the very top. At some point down in the ice sheet, the ice can not be compressed any further. Then it is thinned, due to the flow coming from ice added on the top of the ice sheet and melt at the side of the ice sheet. Like this, thin annual layers of a few centimetres are situated in the lower parts of the ice sheet, whereas the upper annual layers are up to 20 centimetres thick.

For the EGRIP ice core the annual layers have been identified [23] and the age-depth relation obtained (see figure(33)). Thus, information obtained from measurements in a certain depth can be related to a certain time in history.

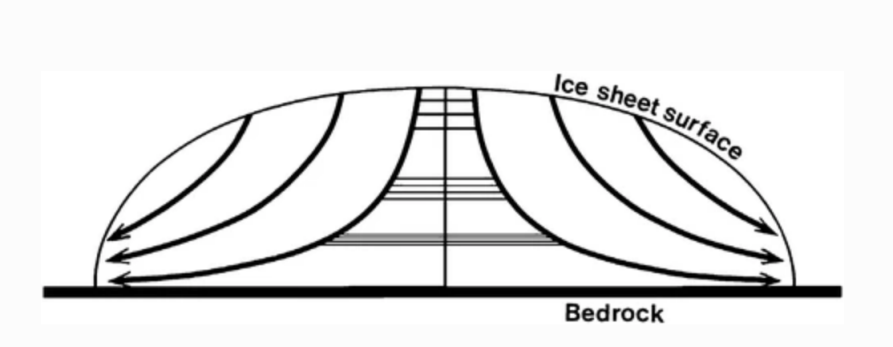

Figure 6: Ice flow and annual layers in ice sheet. (Reproduced from [24])

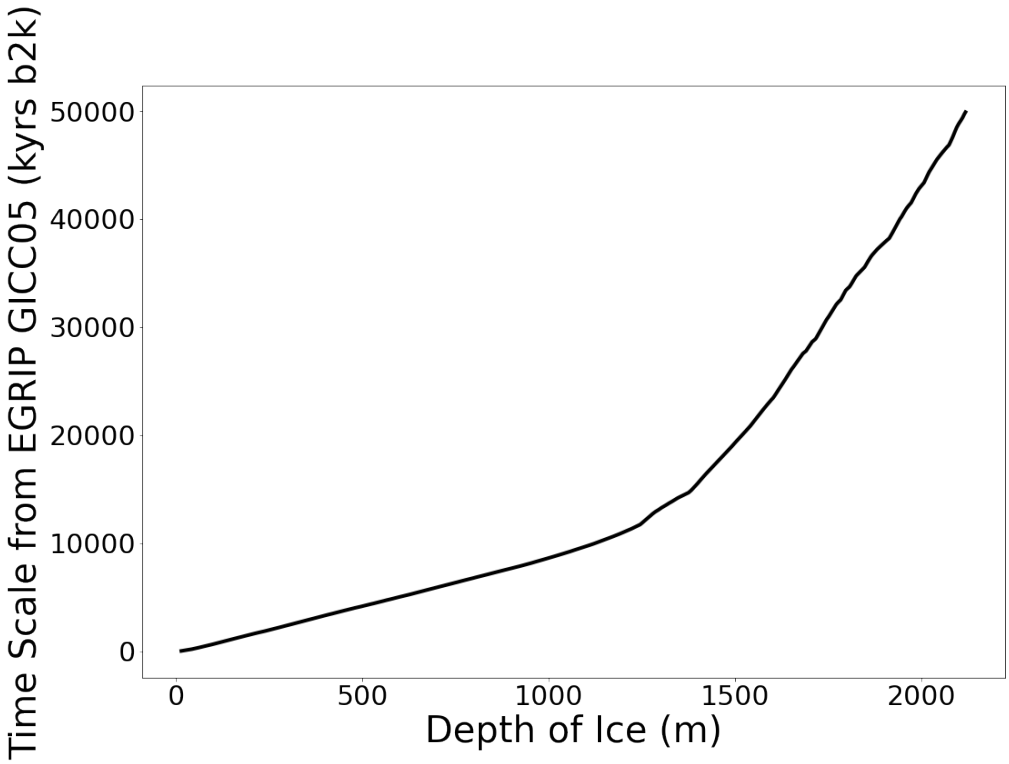

Figure 7: Depth-Age dependency in the EGRIP ice core. (Reproduced from [23])

2.5 Dust in Greenland

With the absence of human activity, the sources for dust 30.000 years ago were saltation, volcanoes and natural burning. These sources were not likely found in Greenland, so the dust must have been transported by the wind and deposited by means of gravity (dry deposition) or snowfall (wet deposition).

2.5.1 Saltation

Saltation takes place in arid areas with sparse vegetation exposing bare soil susceptible to wind erosion. Saltation is a threshold phenomena that occurs due to a complex interaction between dryness, wind and soil surface. Course particles (e.g. grains of sand) bounce in small jumps along the surface and with each impact dislodges finer particles that are suspended in the air and carried away with the wind [21].

Fine particles with less than 70 µm diameter like those observed in the EGRIP ice core are kept aloft by turbulence and can remain in the atmosphere for up to several weeks and may consequently be transported thousands of kilometres downwind [25].

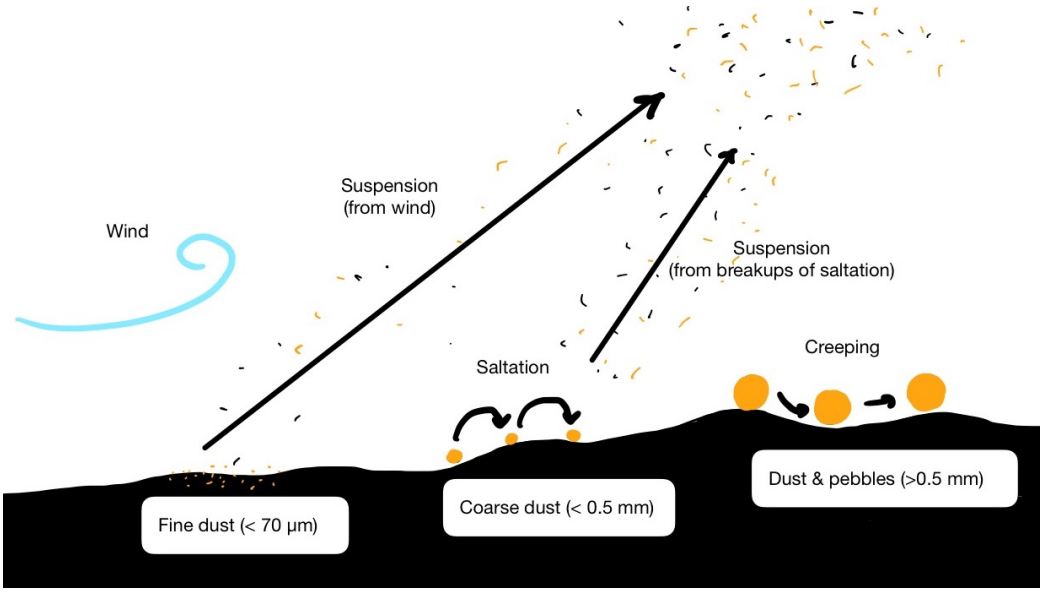

Figure 8: Schematic of atmospheric mineral dust creation due to saltation

2.5.2 Tephra

Volcano ashes - or tephra (greek for ashes) contain tiny glass shards and posses certain electrical and chemical properties that may serve as proxies for their detection in the ice.

Tephra stem from eruption columns that are ejected upwards at high velocity. As air is drawn into it, the density decreases and the material starts to rise buoyantly into the atmosphere. Prevailing winds will then carry the ashes away to be deposited up to thousands of kilometres from the volcano. Coarse particles fall out closer to source and the deposit generally decreases in thickness and grain size exponentially with increasing distance. With volcanoes in Iceland, Alaska and the sea west of Greenland there have been numerous eruptions that may have caused ashes to be deposited on the EGRIP location.

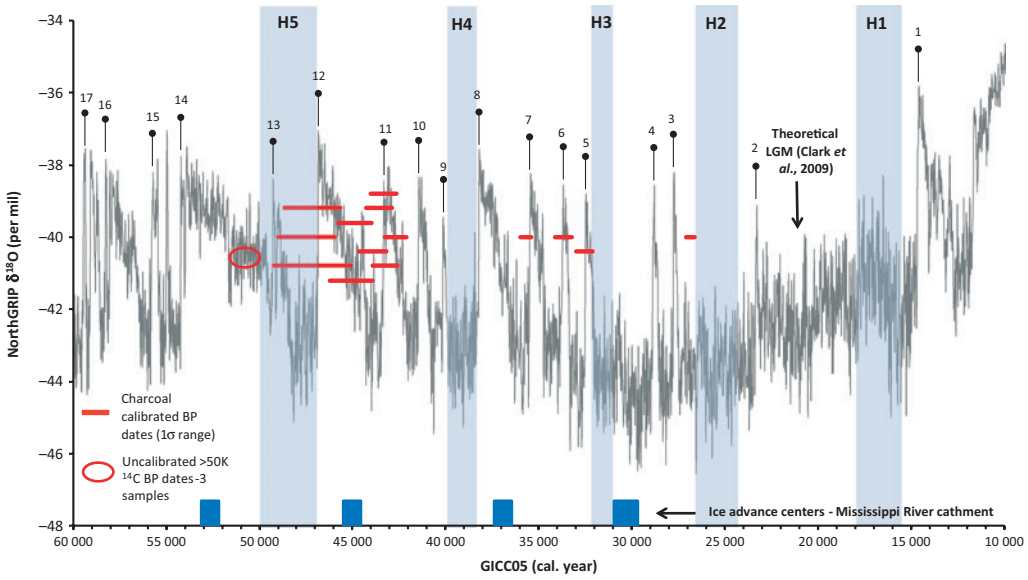

Figure 9: Tephra horizons (Reproduced from [26])

2.5.3 Natural Fires

Smoke from North American forest fires prove to have a high concentration of NH_4^+. Accordingly NH_4^+ plays an important role in a combined fire proxy that may also encompass other fire tracers such as charcoal, levoglucosan and dehydroabietic acid [27].

As with tephra, smoke and ashes from forest fires are carried by the wind and deposited in a similar way. A study of periglacial late Pleistocene fires in central Canada revealed, that fires occurred either hundreds to thousands of years after Dansgaard–Oeschger (DO) interstadial warming events (i.e., the time needed to build enough fuel for fire ignition and spread) or at the onset of the DO event, during stadials. The mechanisms leading to rapid or delayed fires following the onset of DO events were not clarified and the relationship between fires and DO-events were not conclusive [28].

2.6 Influence of Dust on the Climate

Dust plays a key role in the climate system, but the mechanisms are complex and still not understood in all its details. Dust modulates key processes that are inevitably influencing the Earth energy budget [21].

The atmospheric concentration of mineral dust has a major effect on the climate due to its ability to absorb, reflect and scatter sun-rays and so block the radiation energy from reaching and heating the Earth. As a consequence, dust in the atmosphere has a cooling effect on the ground. On Greenland, this is believed to be the most important driver of past abrupt climate changes, such as the Dansgaard-Oeschger (DO) events [21].

On the other hand, dust settles on the ground, where it influences the ability of the surface to absorb or reflect the radiation energy. The ability to reflect the radiation, also known as the Albedo-effect, is especially intense on the ice-sheet, due to its whiteness. Settling dust will weaken this effect, leading to higher energy absorption and thus have a heating effect on the ground.

The emission, transport and disposition of air suspended dust particles forms a complex and challenging system. The transport can be at different spatial and temporal scales depending on particle size and prevailing wind amongst other factors [21]. There are different kinds of active and passive deposition. On Greenland, passive deposition due to gravitational settling, turbulence and snowfall washout must be the dominant ones. Without knowing the spatial-temporal relationship, it is fair to assume that more dust settles at times and places with more dust in the atmosphere and that any time-lag in the deposition is small (and thus ne-

glectable) when compared to the time scale of stadials and interstadials.

Another effect of dust concerns the cloud formation processes. An increase of temperatures means an increase in evaporation of water. As the evaporation increases, more water will eventually condensate into clouds consisting of water droplets, that serve as condensation nuclei and therefore the accumulation of water, so that the rain-/snowfall increases. Dust particles themselves also serve as condensation nuclei and thereby influence the accumulation process. The amount of accumulation and thus the precipitation will in return have an impact on the amount of dry soil and the vegetation due to the rainfall-growth interaction (see figure (10)). As clouds reflect sunlight, they have a cooling effect.

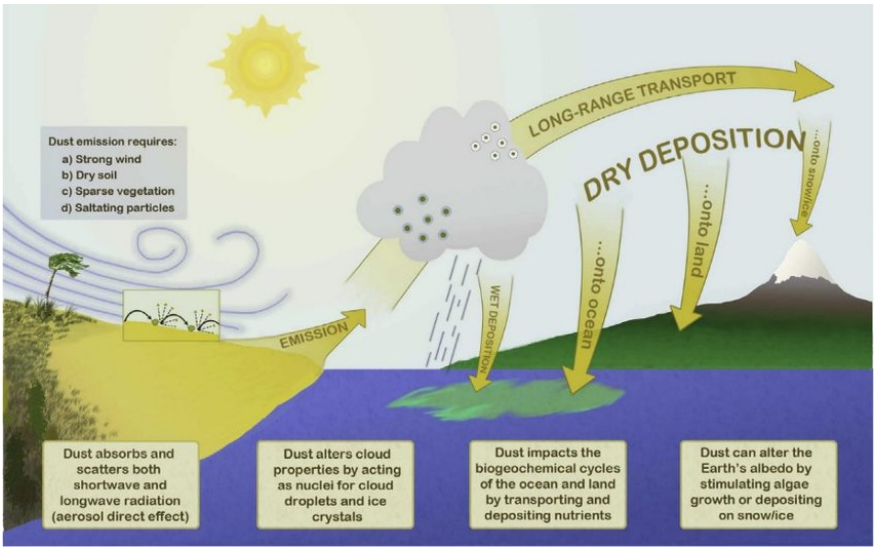

Figure 10: Schematic of mineral dust impacts on climate (Reproduced from [25])

All of this combined with further factors like prevailing winds, temperature, evaporation and the Albedo effect of land, ocean, ice masses and clouds form together a very complex system that determines the weather on a short timescale and the climate on a long timescale.
However, the direct and most influential interaction between dust and temperature remains the reflection, absorption and scattering of radiation due to dust particles in the atmosphere which makes the temperatures sink (figure (11)).

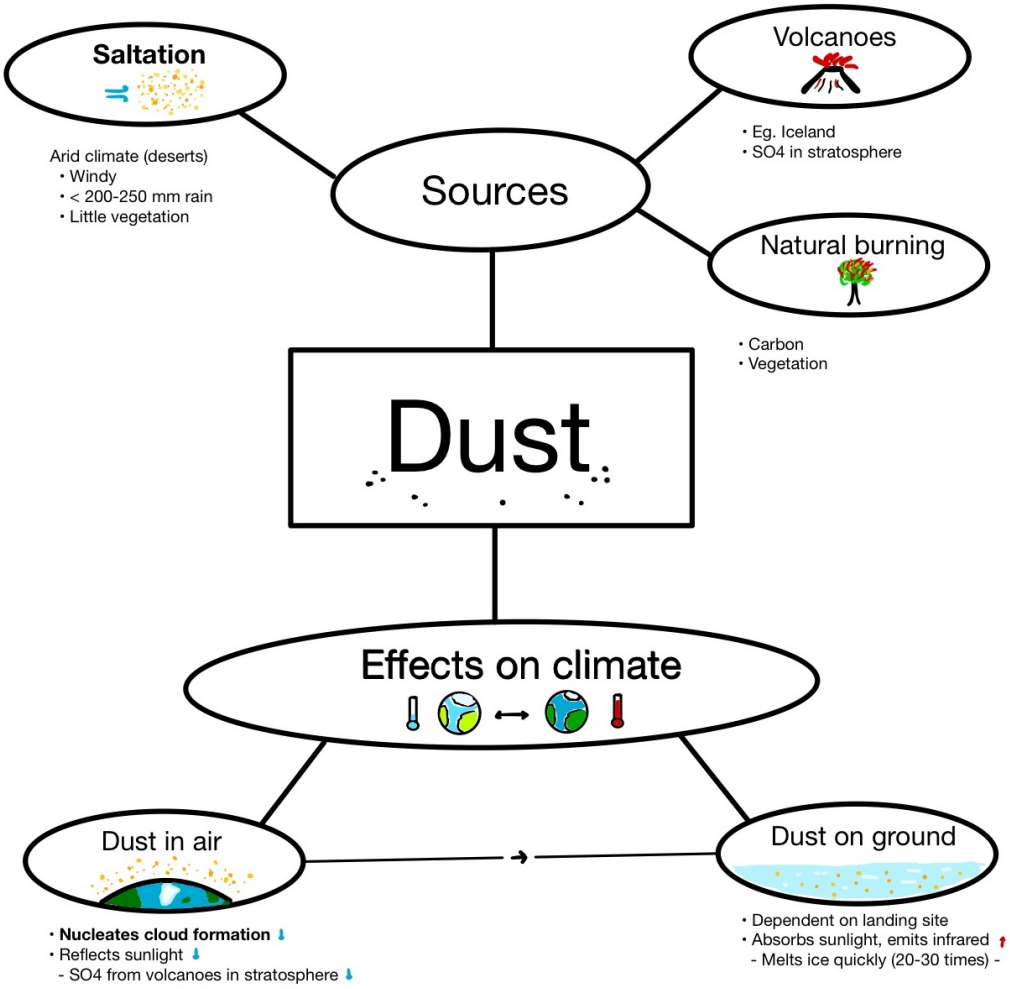

Figure 11: Conceptual overview of Dust-Climate interactions. Small blue arrows indicate a decline in temperatures, whereas small red arrows indicate an increase in temperatures.

3 Methods

3.1 The Ice Bars

The ice from the EGRIP ice core was supplied as 55 cm long bars (also called bags) cut to a square cross-section of 3.5 x 3.5 cm for the gas-measurements according to the EGRIP cutting scheme (see figure (12)).

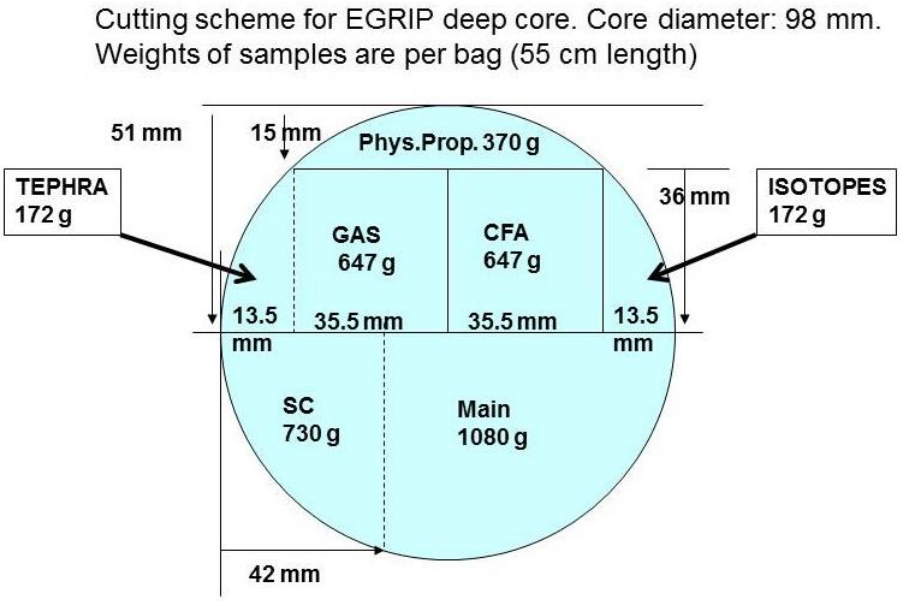

Figure 12: Ice core cutting scheme [3]

In total 346 bars were used for the 'EGRIP gas measurement campaign' covering a depth-interval of ca 216 meters from a depth of 1930 m up to 1713 m. In order to measure the contents of the ice, the bars were melted bottom-up in a deepest first sequence through multiple runs over several weeks, where each run would cover somewhere between 3 and 32 bars and take up to 7 hours.

3.2 The Melting Process

The preparation and melting of the ice took place at NBI in the Continuous Flow Analysis laboratory (CFA Lab). The practical work consisted of feeding the ice to a melting process and monitoring and controlling the melting and data collection process. This work is usually performed in runs by two to three people present in the lab.

The setup is quite simple. The ice-bars are first prepared with the saw and then melted bottom-up on a melt-head (see figure(13)). Tubes lead the melting-stream from underneath the melt-head to different instruments that all fulfil their respective tasks. The first instrument is the de-bubbler. The de-bubbler serves to eliminate air bubbles in the melted ice. These

bubbles could otherwise be mistaken as dust particles in the ice later on. The de-bubbled water is now pumped to the ABAKUS apparatus. This device counts the amount of dust particles in the melt-stream per second in various dust-size classes. Also, the flow of the melt-stream is measured by a flow-meter. It measures in ml per minute how much melted ice is flowing through the system. Further properties of the melted ice are measured which won't be discussed any deeper in this thesis. Finally, a computer connected to the different instruments monitors the melting process and gathers and saves all the data.

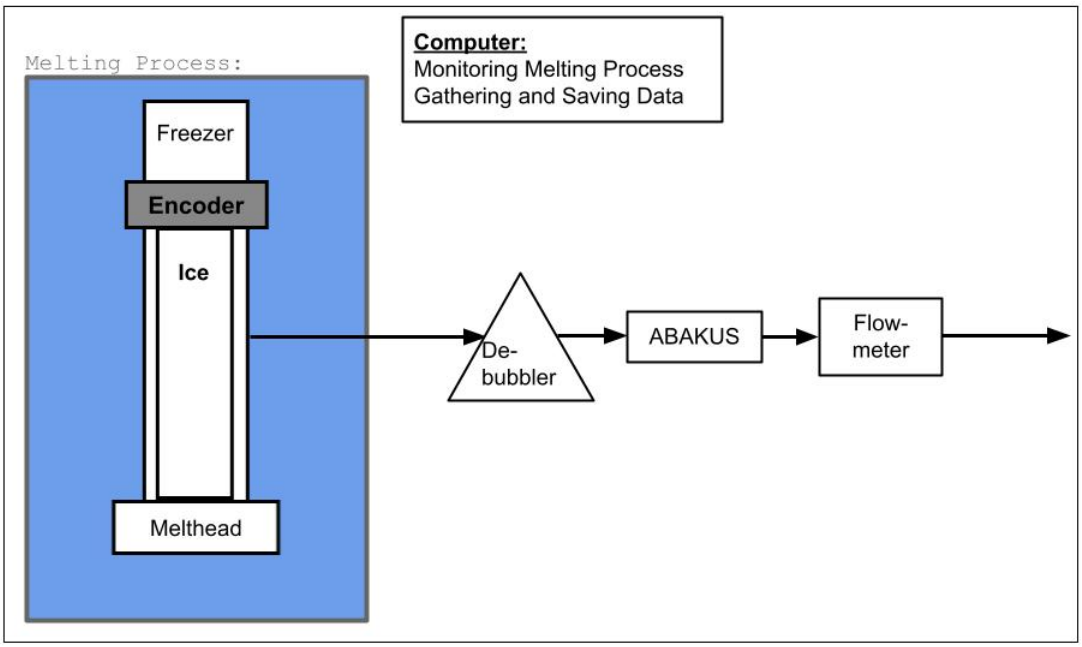

Figure 13: Experimental setup in the Laboratory

In the following, the process will be explained more to detail: Before the process starts, the originally 55 cm long ice-bars are prepared for melting by cutting away the sections that would pollute or otherwise complicate the measurements. These are typically at the ends or where breaks appear in the ice and thereby pose a risk that air can come in between two parts of ice. For each bar these cut-offs representing missing ice were documented in a cutting sheet. The prepared ice-bar is then placed in a pre-arranged plastic framework, that later on holds the ice-bar in the melter frame in an upright position. The bottom of the ice-bar is situated on the melt-head. This melt-head is a thick metal block with five holes. It is warmed and

thereafter the melted ice flows through the bottom holes. In order to avoid any contamination, possibly occurring on the surface of the ice bar, the melt-head's outer four holes lead to waste, whereas the hole in the middle lead to the measuring instruments (see figure(14)).

Figure 14: Photo of the melt-head with draining holes. Outer four holes are for fixation, only.

On top of the ice a weight is placed, that presses the ice down towards the melt-head. A linear position encoder fixed to the weight measures

[25 steps/mm] the deescalation of the bar by the second (see figure(13)). When there is about 12 cm left of the melting ice-bar, the encoder is detached and the weight lifted off to allow for the next ice-bar to be stacked on top of the previous one. This usually takes around 1 minute in which the encoder shows a constant low value. The weight is then applied to the new bar and the encoder is again attached to the weight. Each cycle lasts between 10 and 14 minutes. Under the first bar and on top of the last bar in a run, small ice-bars of ultra-pure water (Milli-Q or Mq after the water purification system) are added in order to rinse and calibrate the instruments. Figure (15) illustrates the principles of the process from the preparation of the ice-bars to the resulting encoder-value recording during the melting.

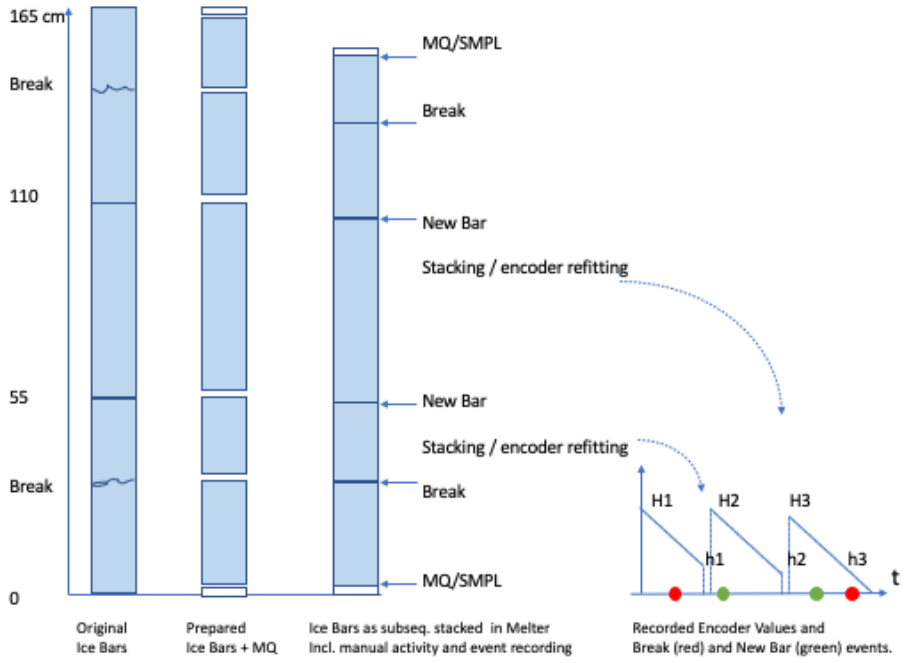

Figure 15: Principle: Preparing, Melting and Recording

Figure (16) shows the obtained encoder values for a run over almost 3 hours in which 12 bars were melted. The square box marks the part of the run with real ice, i.e. without Mq-ice.

The encoder-values for the melt-down positions are recorded together with the dust count and some measurements from the other instruments in one file for the complete run. In a second file (the ABAKUS file) the detailed dust counts in 32 size classes are recorded. The sampling period for both files is one second, so we have a one to one correspondence between the file records. Also recorded along with the encoder-values is the information, if Milli-Q ice or the EGRIP ice-samples are melted ('MQ/SMPL'), as are the events 'New bag' and 'Break' whenever a new bar or a break in a bar hits the melting-head (shown in fig(16) as green and red dots, respectively). For every run, the cutting sheet information for the bars of the run were recorded in a corresponding cutting-sheet file.

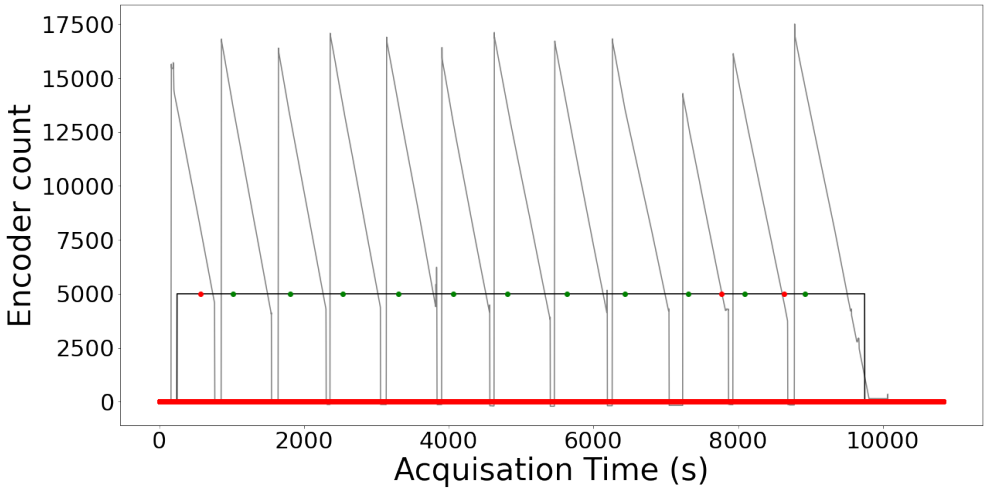

Figure 16: Encoder graph for Run 3460 containing 12 bars. (Encoder graph in grey). Green points indicate New bag events, whereas red points indicate breaks. The Mq_smpl index is marked by a black bar.

3.3 Data Processing

The data processing was done in a Python programming environment, that was also used to produce most data plots used in this thesis. The program code was developed specifically for early processing of the available data-files and for flexibility of experimental usage. Classical objectives such as scalability, re-usability, modularity was not pursued. The essential program functions are supplied by link in the appendix.

3.3.1 Setting the Data on a Depth-Scale

Setting the data on a depth-scale basically means calculating and adding depth-values to the data-sets containing the encoder- and measurement-data. For this purpose two sets of information are used: 1) The numbering sequence of the ice-bars of known length and 2) The position-encoder values of the measurement records. In more detail, the process involves the original bar length of 55 cm, the bar-number, the elapsed time, the encoder-positions of the 'New bag' and 'Break' events, the cutting-sheet information for these events, the encoder-values themselves and the MQ/SMPL information.

The numerical processing goes through the following steps for each run:

1. Filtering out the data of the Mq-ice based on the MQ/SMPL recording
2. Identifying and repairing the invalid intervals of the encoder-value records. Those are any interval, where the encoder might have stuck and the intervals, where the encoder was refitted during stacking of the next bar.
3. Elevating and connecting the encoder-lines to form one long line for the run
4. Adjusting for the cuts
5. Off-setting all values of the run to match the starting point with the original ice-depth of the first bar of the run.

Ad 1): Filtering out the data of the Mq-ice is simple, since Mq-ice always and only occur in the beginning and in the end of a run. The Mq-ice records are ignored.

Ad 2): The encoder-values basically form a series of declining slopes when put into a graph with some noise between the slopes, deriving from where the encoder is detached and refitted. The start- and end-points of each encoder-slope (Hn and hn in figure (15)) are determined by applying slope and slope-change constraints that identifies the points of abrupt change in encoder values. Encoder values lying outside or in between the encoder slopes are ignored (deleted). Figure (18 and 19) shows an example of the encoder-values in a line plot with and without point-markers. In these

plots you can easily identify some high values resulting from the over-stretching of the encoder being re-fitted to a new bar. Also the low values, occurring through detachment and relaxation of the encoder during the stacking of a new bar are clearly visible in the plots.
Next, any portions within the encoder-slopes, where the inclination locally gets near zero are identified. Such situations occurred up to 5 times per run whenever the encoder gets temporally stuck due to mechanical problems. The start- and end-point of every such occurrence are identified and the encoder values of the involved portion are replaced by fitting a straight line connecting the two points (see figure (21)). The exact criteria for the constraints were found experimentally/visually through several iterations and is documented inline in the source-code. In order to close the gaps between the encoder-lines (i.e. the time where the encoder was detached and re-fitted), the lower end of each line is extrapolated over the time of the gap (see figure (15 and 23)).

Ad 3): The encoder-lines are individually off-set, so that the last value of one line aligns with the start value of the next line, resulting in one long line for the whole run, as if we had a "global" encoder, long enough to stretch over all the bars of the run (see figure (24)).

Ad 4): The modified encoder values are converted into cm, using the conversion factor 25 units per mm (see figure (25)). Next the encoder line is processed to incorporate the size of the cuts stemming from the preparation of the bars. At every 'New Bag' or 'Break' event position, the cutting sheet information is used to lift the encoder line by as many cm as the gap produced by the cut (see figure (26)). As a result the depth span of the encoder line [cm] should match the sum of the original lengths of the melted bars.

Ad 5): Finally, the modified encoder values are all given an off-set, so that the first value matches the depth of the bottom of the deepest bar (first ice on the melter) (see figure (27)). This depth is calculated by multiplying the bag-number of the bar by 55 cm.

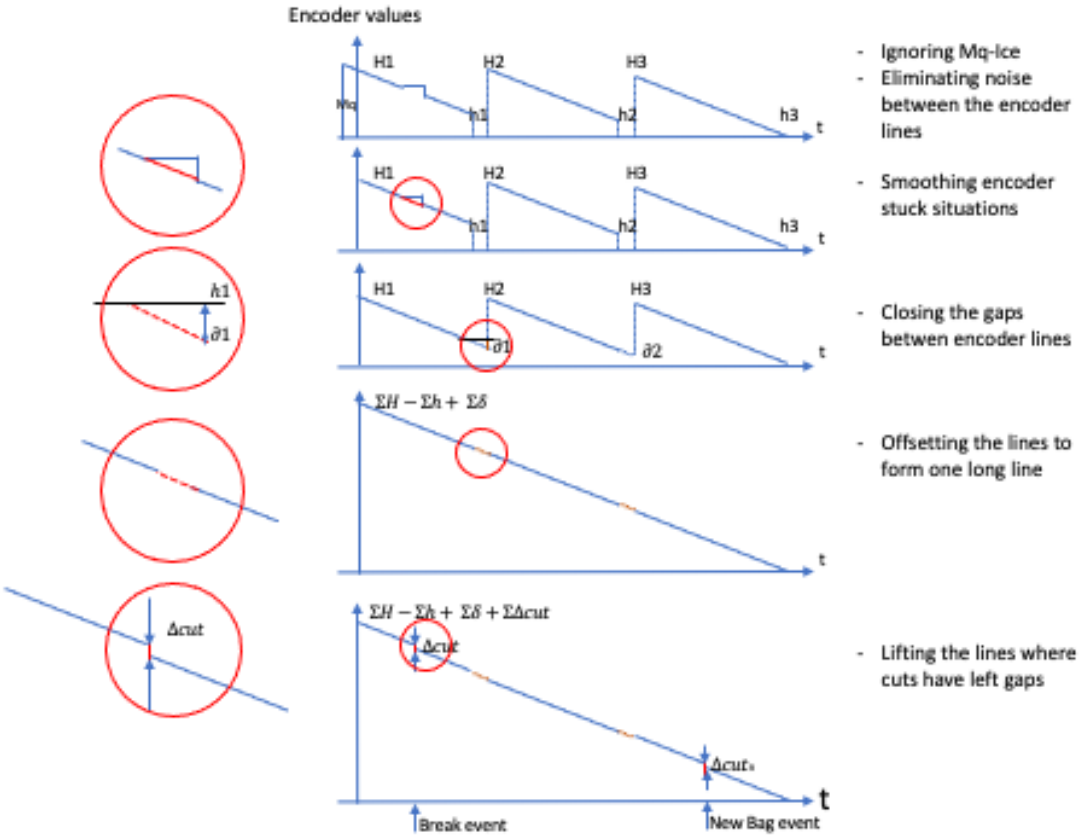

Figure 17: Encoder Value Processing principle

The following plots show step by step the results of the encoder value processing for a specific run over 12 bars as an example.

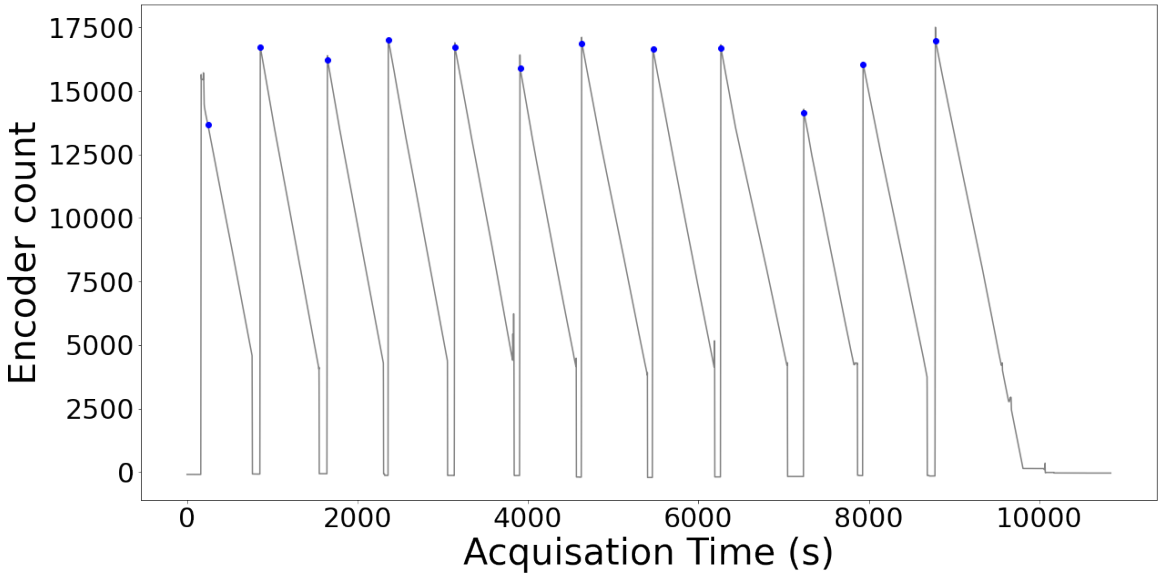

Figure 18: Example: Encoder line plot with identified starting-points of each slope

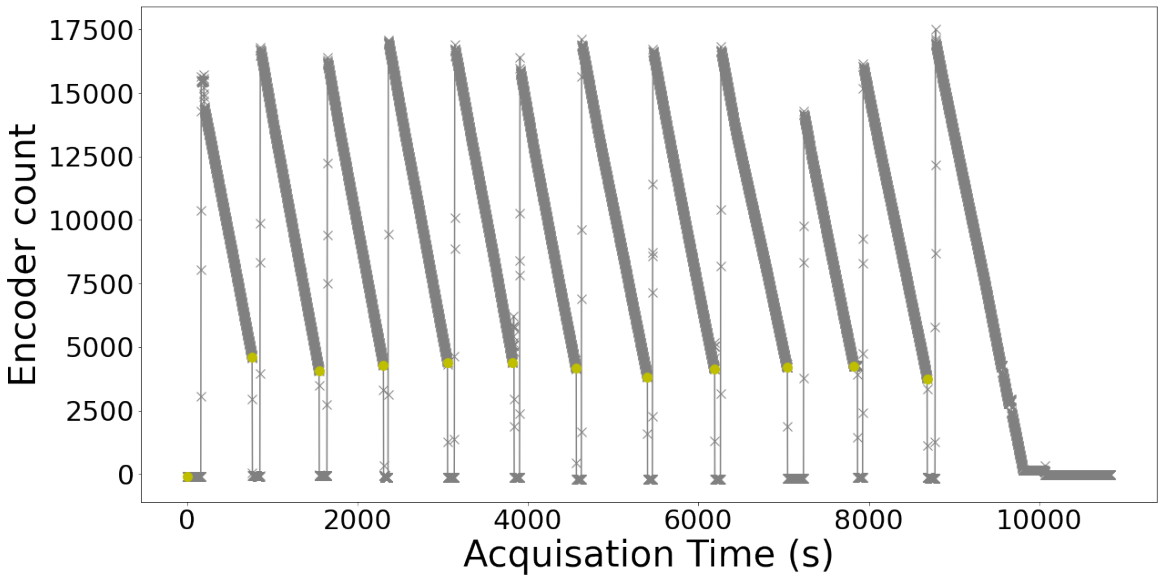

Figure 19: Example: Encoder line and marker plot with identified end-points of each slope

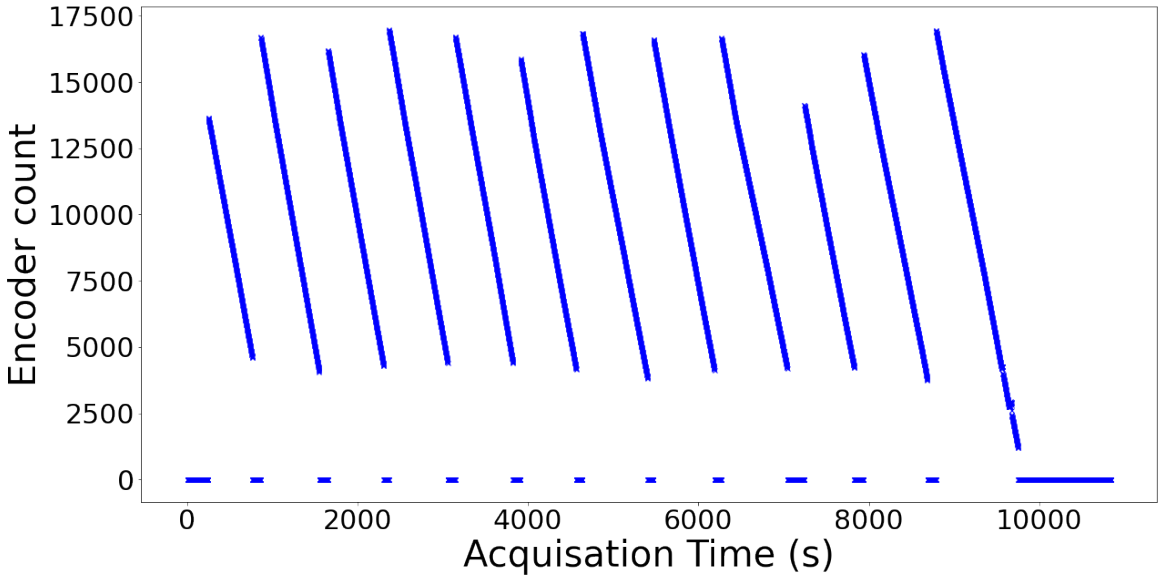

Figure 20: Example: Encoder marker plot after 'noise' removed

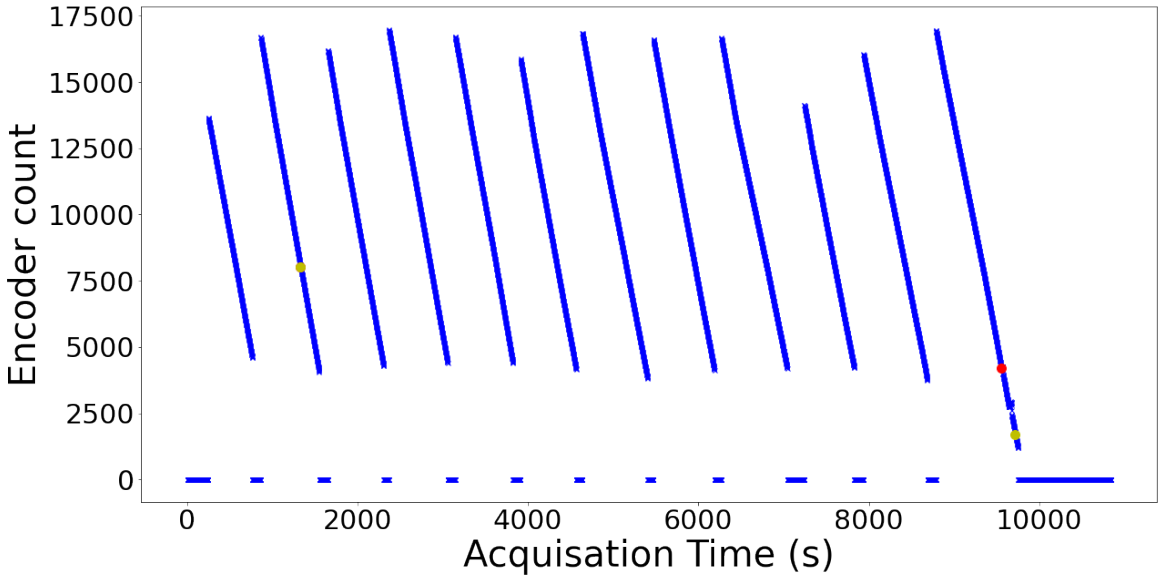

Figure 21: Example: ... with identified encoder-stuck situations in second and in last slope

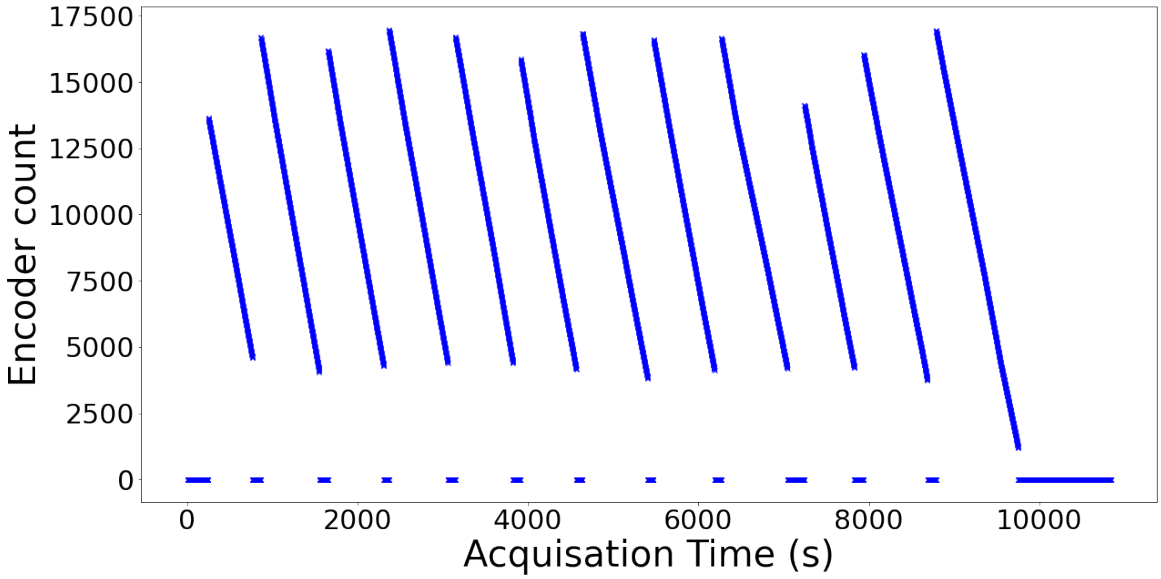

Figure 22: Example: ... with smoothed encoder stuck situations in second and in last slope

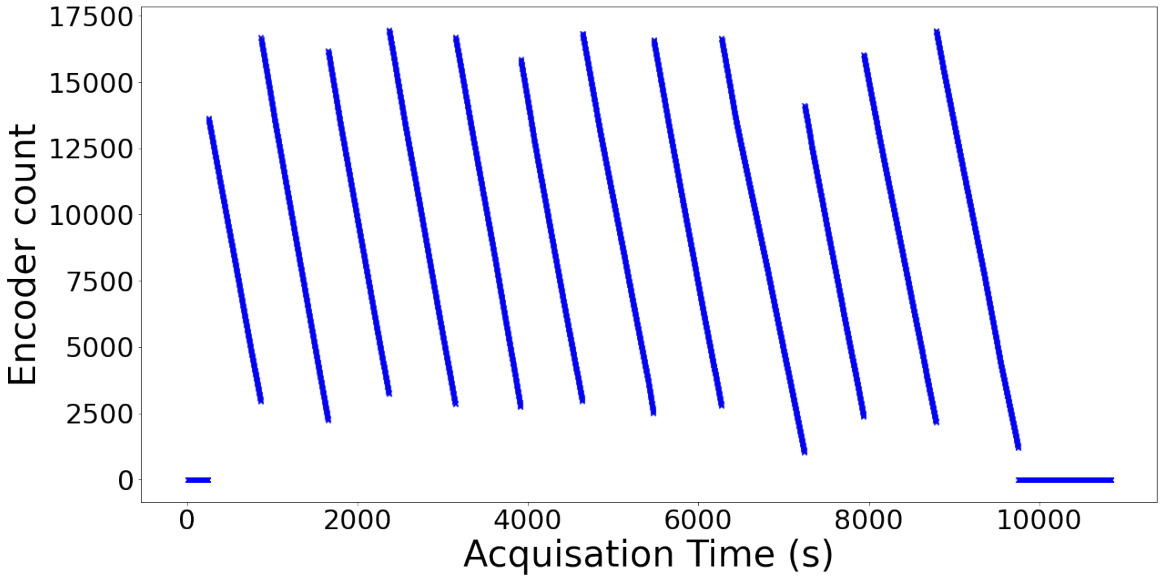

Figure 23: Example: ... with slopes extrapolated to close the gaps where the encoder was detached and values otherwise zero

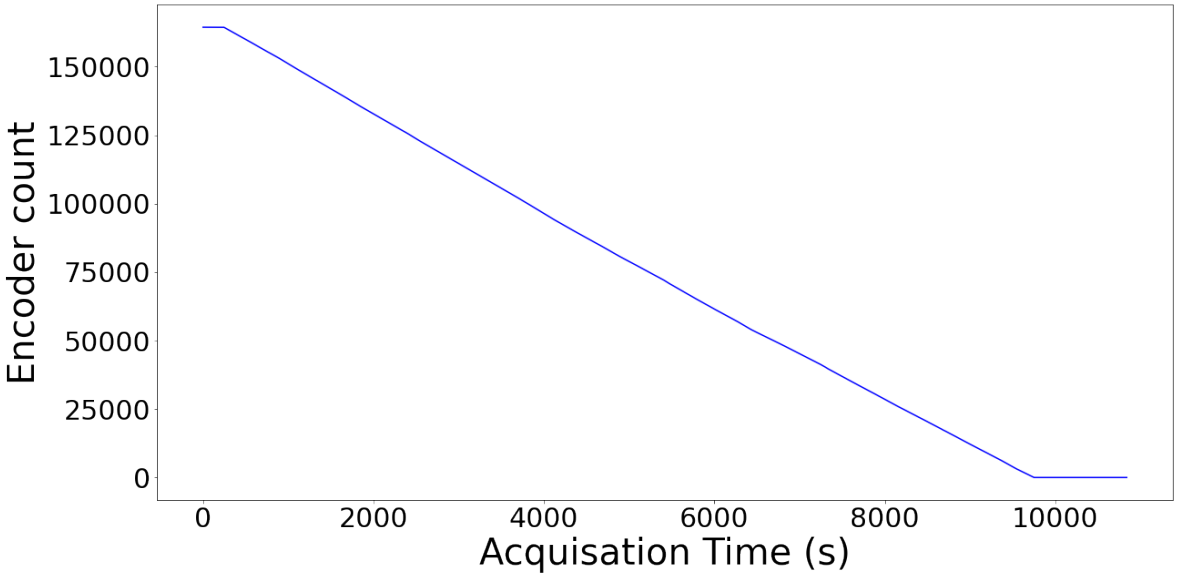

Figure 24: Example: Encoder line plot with slopes individually off-set to form one long slope

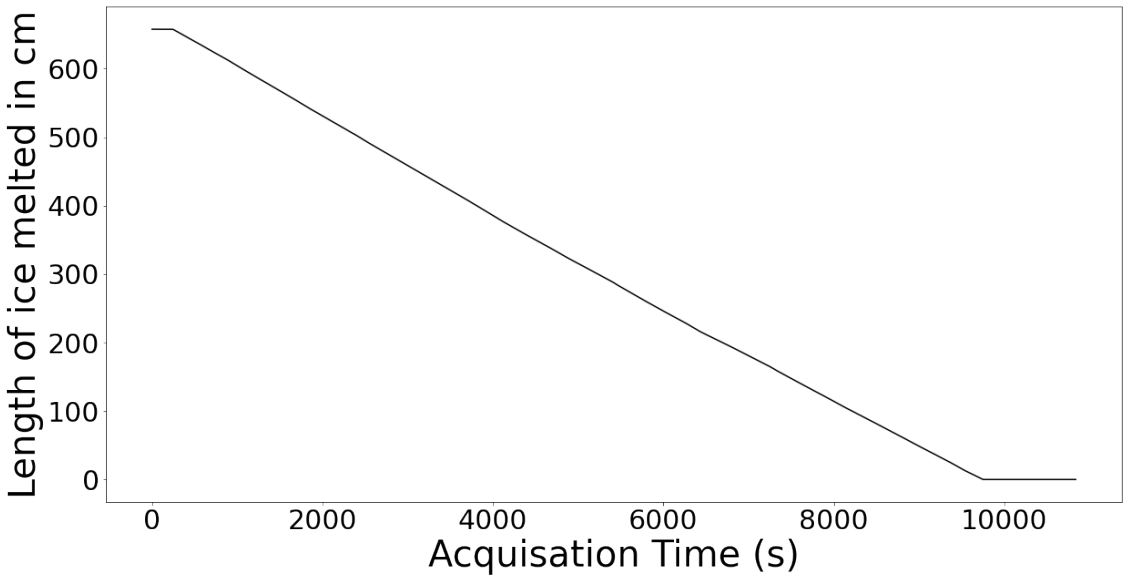

Figure 25: Example: ... with encoder values converted to cm ice

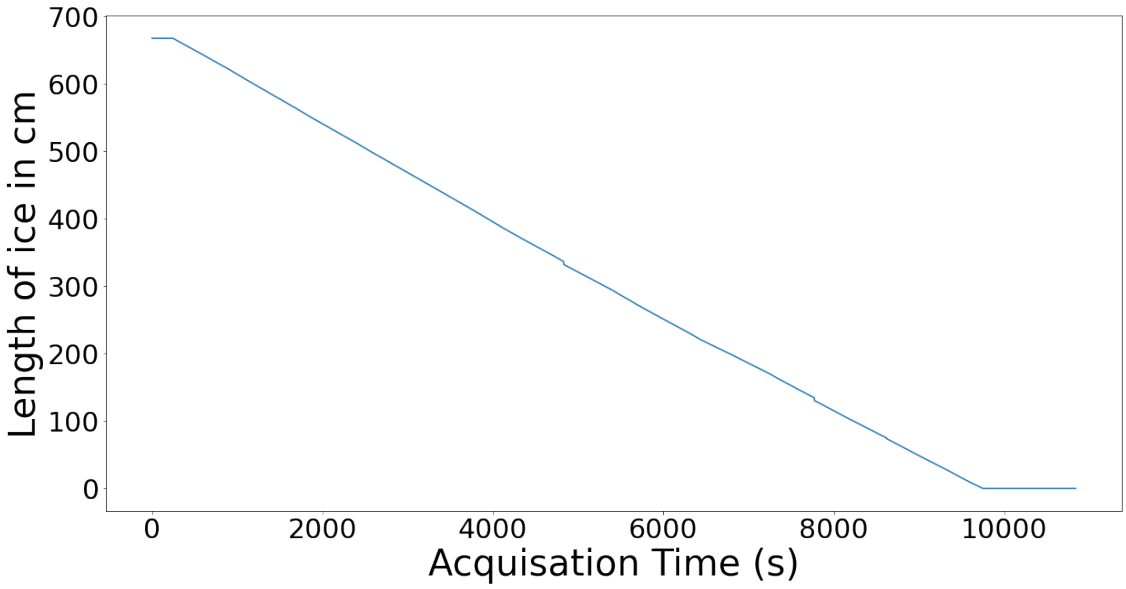

Figure 26: Example: ... with adjustments for ice-cuts (visible only around second 4800 and 7800)

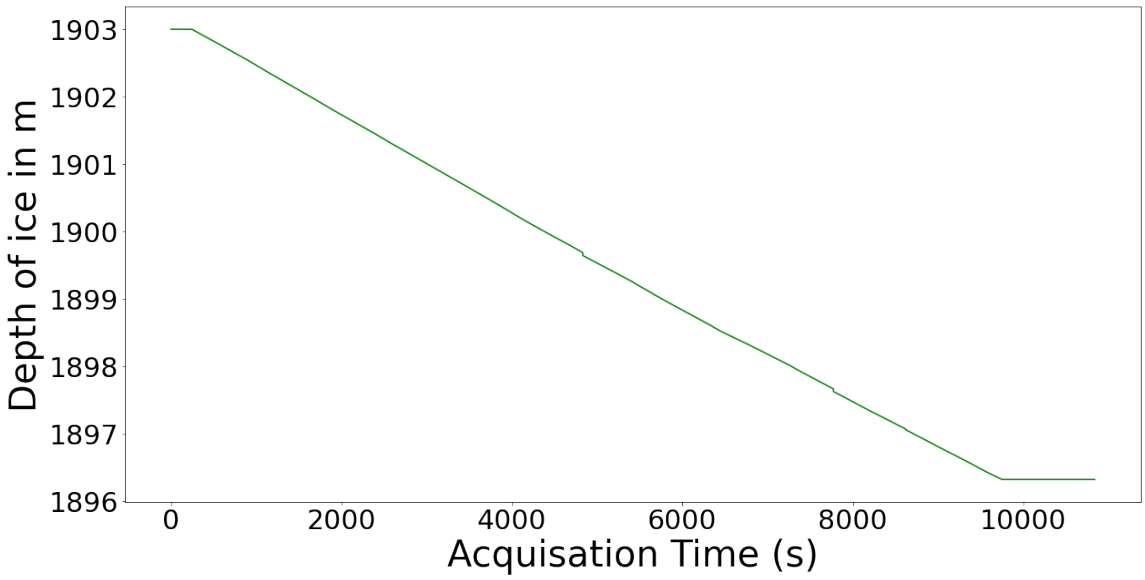

Figure 27: Example: ... with cm ice values converted to absolute depth [m]. The run started with bar 3460 in depth 1903 m

As a first result of the preprocessing, the dust records are set on a depth scale and can be visualised in a scatter plot shown in figure (28).

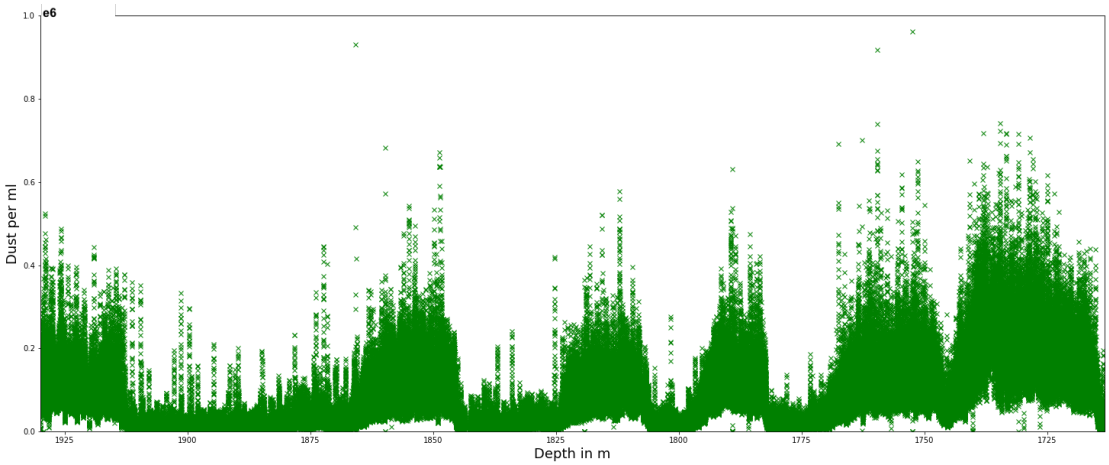

Figure 28: Dust counts per ml over the depth of melted EGRIP ice.

3.3.2 Setting Data on a Timeline

Calendar dating of the ice has been made for different core drillings in different depths. Relevant for this thesis, are the depths below 1725 m. For calendar dating, various techniques may be applied, - often in combination. The techniques range from layer counting wherever seasonal variation allows (typically in the upper layers) to measurement of distinct radioactive, chemical, electrical or mechanical (e.g. dust) properties, that may be related to known events or otherwise belonging to a certain age.

For the depths below 1725 meter, the GICC05-EGRIP-1 time scale (see [23]) is based on ECM-matchpoints (electrical conductivity measurement) between EGRIP and NGRIP2 (patterns, peaks and dips), establishing the depth–age relationship of the EGRIP ice core. The calendar dating of the NGRIP2 for 14.7-41.8 ka b2k (see supplement to [29]) was based on multi-parameter counting of annual layers and alignment with other time scales as described in two papers (see [30] and [31] for details).

By means of interpolation, the GICC05-EGRIP-1 time scale has a resolution of 55 cm, matching the length of the ice bars. The Maximum Counting Error (MCE) amounts to a value between 930 and 1485 years for the relevant depths between 1725 and 1925 meters, witch relative to the age amounts to 3 to 4%.

By use of the GICC05-EGRIP-1 time scale the dust-measurements for this paper was transformed from the depth scale to an age scale.

3.4 Resolutions

This section treats the topic of resolutions and gaps of the depth- and age data obtained and presented in this paper.

The sample period of the data records was 1 second and the melt-down was somewhere between 0.5 and 0.7 mm/sec. After the preprocessing and putting together the data from all the runs as described in section 3.3, we check the resulting sequence of measurements presented in the depth-plot (figure (28)).

The plot presented in figure(29) shows the difference of the calculated depth between subsequent records. For the majority of the records, this difference lies between 0.5 and 0.7 mm corresponding to the speed of melt-down (see figure(30)). In the corresponding plot of the differences of age of the ice between consecutive records (fig. (31)) we have a similar situation. Most age points are distanced from each other by ca. 0.0315 years throughout the whole dataset. This is the temporal resolution of our data (see figure(32)).

There is however, a number of outliers to both sides. A few big gaps between two consecutive records are due to missing or left out ice. The most prominent example is a ca. 30 years gap near record 120,000 (see figure(31). This is because two cores were not taken into the calculations due to computational difficulties. This also corresponds to a gap in the depth points of about 1 meter.

There are also a few positive differences (above the x-axis) between consecutive records, that theoretically should not be there, since the ice melt-down was not reversed (ice melted and then refrozen and then melted again). Also, multiple dust measurements should not overlap in the order of measurement. These positive differences may be due to errors in dealing with breaks and new-bag events or due to possible boundary effects, when putting the data from different runs together. They are, however of little magnitude (max. 8 years), so that they don't have a significant impact on our final results.

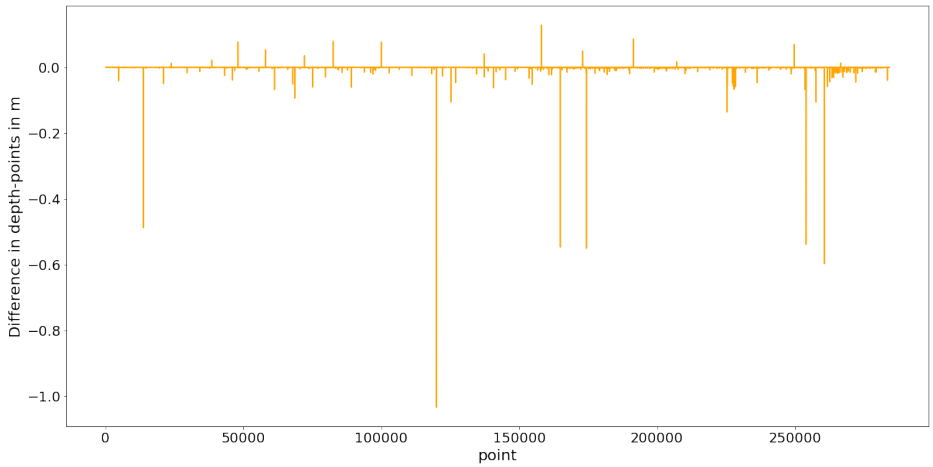

Figure 29: Depth difference between consecutive records

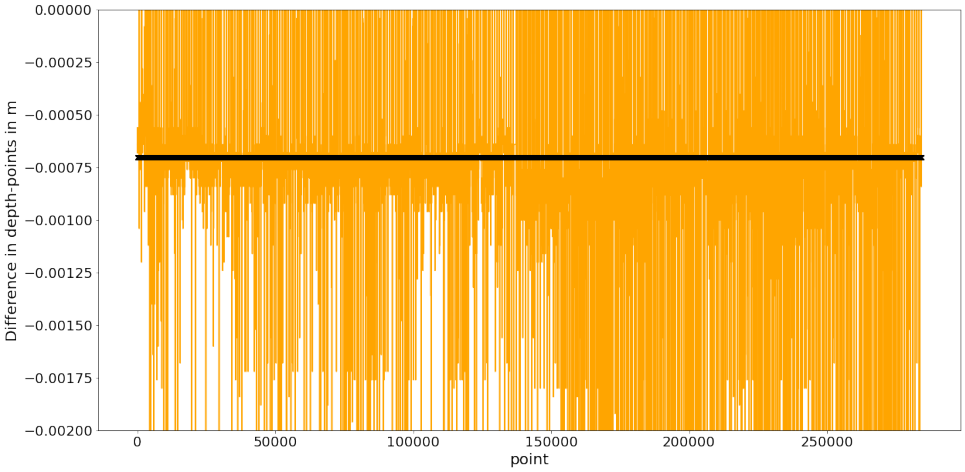

Figure 30: Zoom on the plot from figure(29). Black line is a best guess on the average depth distance. It is situated at -0.0007 m

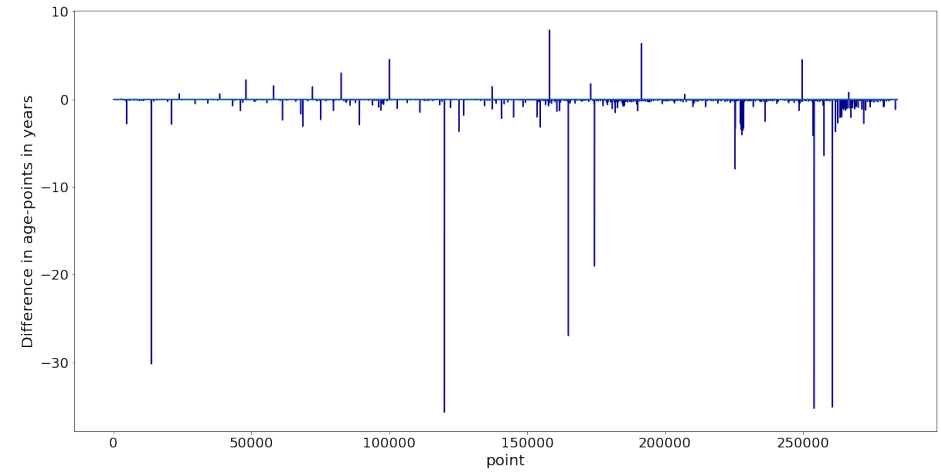

Figure 31: Age difference between consecutive records

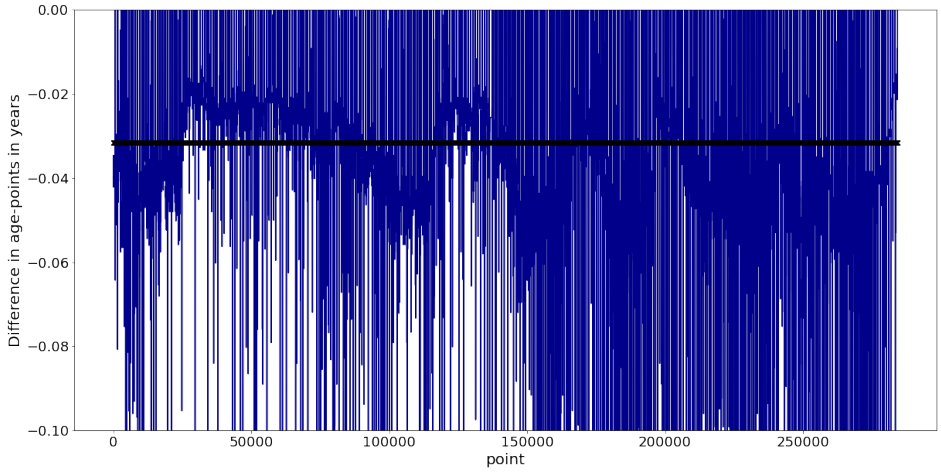

Figure 32: Zoom on the plot from figure(31). Black line is a best guess on the average age distance. It is situated at -0.0315 years.

The reason for the more or less constant age-resolution throughout our dataset is the fact that in the time range we investigate, the depth-age relation is almost linear. Figure(33) shows an extract of the age-depth plot from figure(7). The graph is made up of many points for the relevant time range from about 29,000 years b2k to about 39,000 years b2k. The plot in

figure(34) shows that the interpolation procedure used to assign age to every record was correct as it shows the depths and corresponding age that we arrive at in our code. It can be seen, that there are many more points and that these were interpolated correctly, as they are allocated in between the points from the function that it was interpolated of.

From the plot in figure(33) we see that the 200m correspond to ca. 9,000 years. This corresponds to 45 years per meter ice. Since the GICC05-EGRIP time scale file [23] is based on only ca. 60 NGRIP match-points for this depth-interval (with in-between interpolations to bag-length) and the maximum counting error (MCE) grows from 930 to almost 1500 years (i.e. 3 - 4 %) for the relevant interval, the fine resolution of our data does not say anything about the precision of the age determination of the ice.

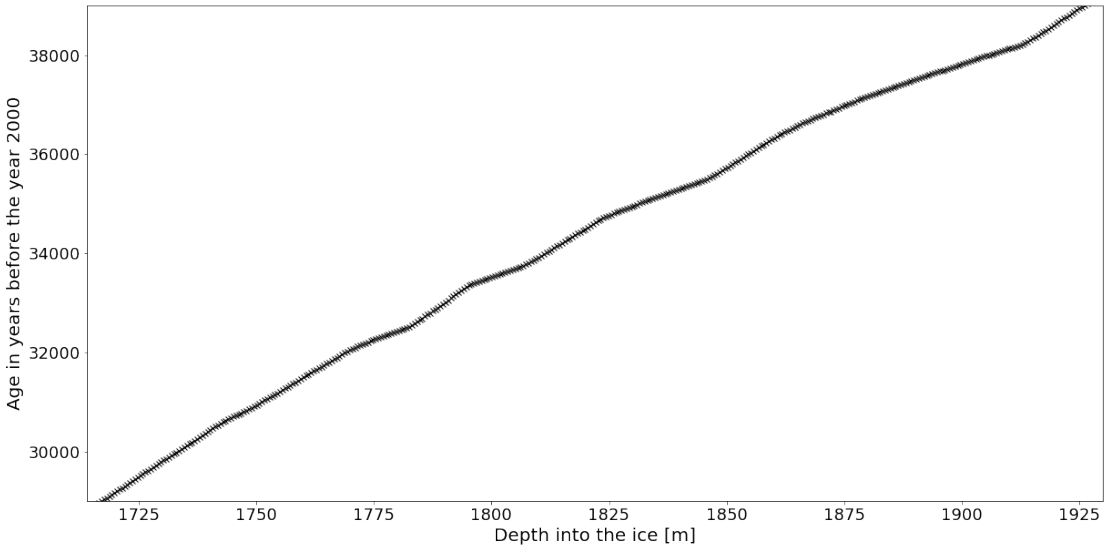

Figure 33: This figure shows the age-depth relationship from the GICC05 EGRIP time scale file ([23])

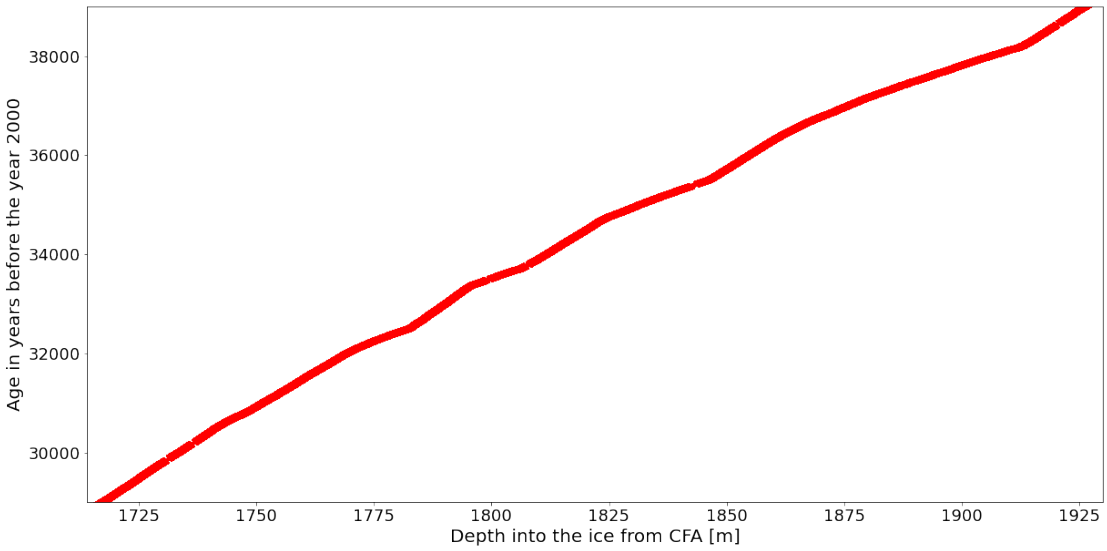

Figure 34: Depth-age relationship after adding interpolation point to match the depth resolution of our measurements

3.4.1 The Flow of the Melt-Stream

The flow recordings are used in order to transform the dust count per sample to dust count per ml melted snow. Since the flow is recorded as [ml/min] the formula is simple:

$$dust[count/ml] = dust[count/sec] * 60[sec/min]/flow[ml/min] \quad (1)$$

The quantities and quality of the flow-measurements was briefly examined and some anomalies found.

The average flow measured is just below 1 ml per minute which is just a fraction of the melted volume of roughly 40 ml per minute (the typical encoder diff of 14 counts and the resolution of 25 counts per mm gives 14/25 = 0.56 mm/sec which multiplied with the cross-section (35x35 mm^2 gives 686 mm^3/sec or $\approx$ 40 ml/min).

When looking in detail on the flow-values some outliers can be identified. E.g. for the very first run in which 3 bars (3509 to 3506) were melted (see figures (35 and 36)), a dip with a duration of 3 sec occurred 18 sec after a new bag event and a significant (double-)peak with a duration of 8

sec occurred 52 sec after the same new bag event. Finally, a much smaller peak occurred towards the end of the run around 6 sec before the MQ was recorded. Also the run starting with bar 3491, 3479, 3147, 3195 had outliers (one peak each). In 3147 something went wrong in the MQ part. If, and possibly how these flow outliers actually are related to the events could not be verified. When looking at the dust counts, many dips and peaks occur (as we shall examine later). However, non of these seems in any way correlated to the outliers of the flow measurement. One explanation for outliers could be swift obstructions of the flow (e.g. through ice) or errors in the flowmeter-measurements and not in the flow itself.

When looking closely at figure (36) also a distinct oscillation of the flow may be observed, that occur when two sine waves with the same amplitude and a small frequency difference are superposed. The resulting wave exhibits the average frequency (ca. 1/3 Hz) and a slow amplitude modulation (ca. 1/100 Hz) caused by the frequency difference of the two waves. This phenomena may well originate from a small speed difference of the two pumps involved. In run 3195 the amplitude of the oscillation switched for unknown reasons multiple times between two distinct sizes. Since the amplitudes are relatively small compared to the average flow, the oscillation phenomena is generally ignored.

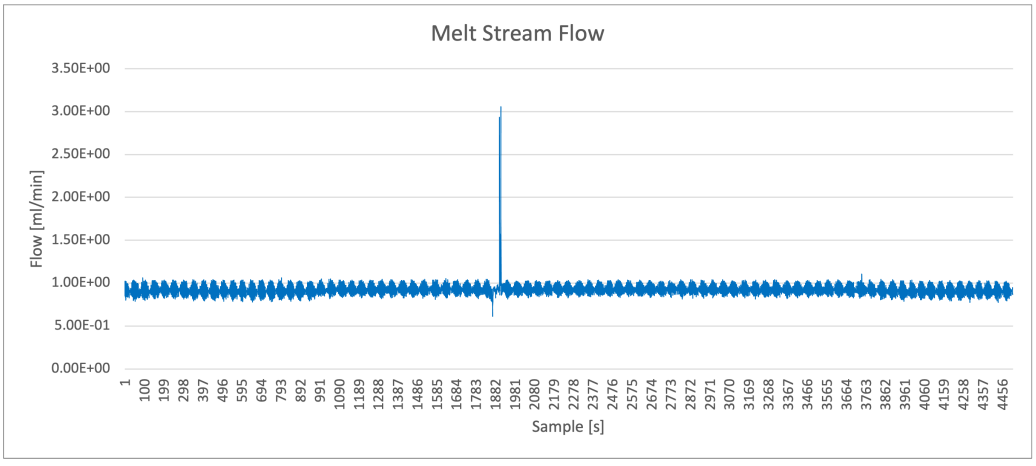

Figure 35: Example: Flow for run 1 (bars 3509 to 3507

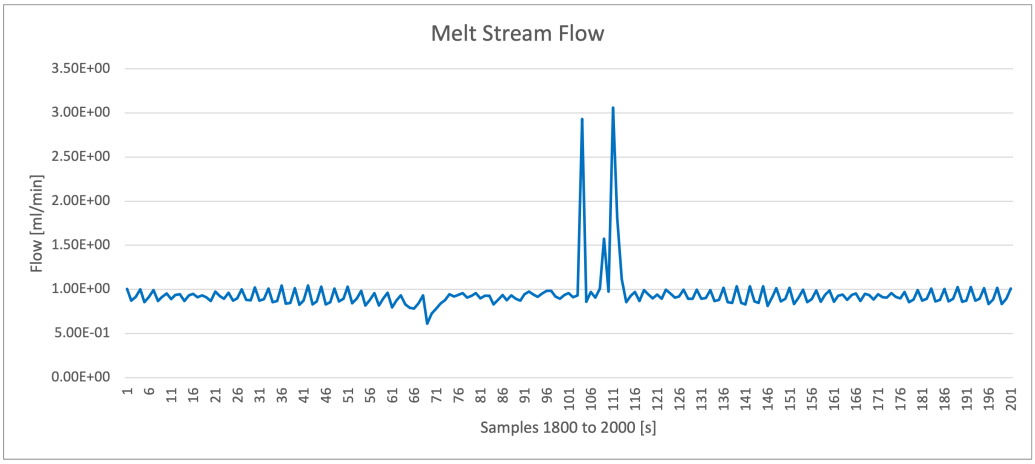

Figure 36: Example: ... with interesting section enhanced

3.4.2 Categorise Data

The dust size counts were collected for each run in ABAKUS-files. The sampling-period was 1 sec, matching the sampling in the corresponding encoder-files. The dust particles were counted in the size bins: 0.8, 0.9, 1.0, 1.1, 1.2, 1.3, 1.4, 1.5, 1.6, 1.7, 1.8, 1.9, 2.0, 2.1, 2.2, 2.3, 2.4, 2.5, 2.8, 3.2, 3.6, 4.1, 4.7, 5.4, 6.1, 6.9, 7.9, 9.0, 10.2, 11.6, 13.2 and 15.0, where the numbers refer to the particle diameter in µm. The two small-particle bins (≤ 1.0 µm) are discarded since their measurements are too noisy, presumably due to counts of small air-bubbles surviving the de-bubbler. The sum of the > 1 µm particles of each sample was also recorded in the encoder-file.

Due to a gradual step up in bin-widths above the 2.5 µm bin, the counts in the different bins are not comparable (see figure (37)). In order to visualise the distribution of dust-particles with regard to size, the counts of each bin is divided with the bin-width as shown in figure (38). Using this kind of normalisation allows for a comparison of dust distribution with regard to size over time, e.g. over different stadials.

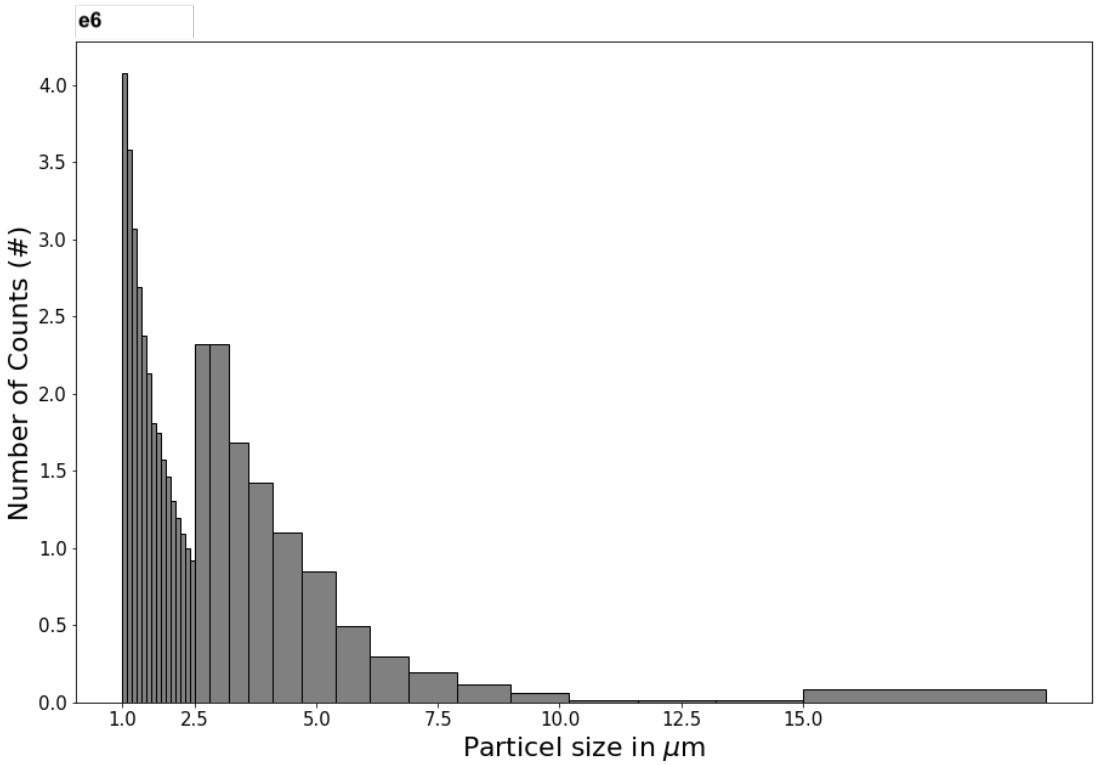

Figure 37: Example: Dust distribution in size-classes with different bin-widths

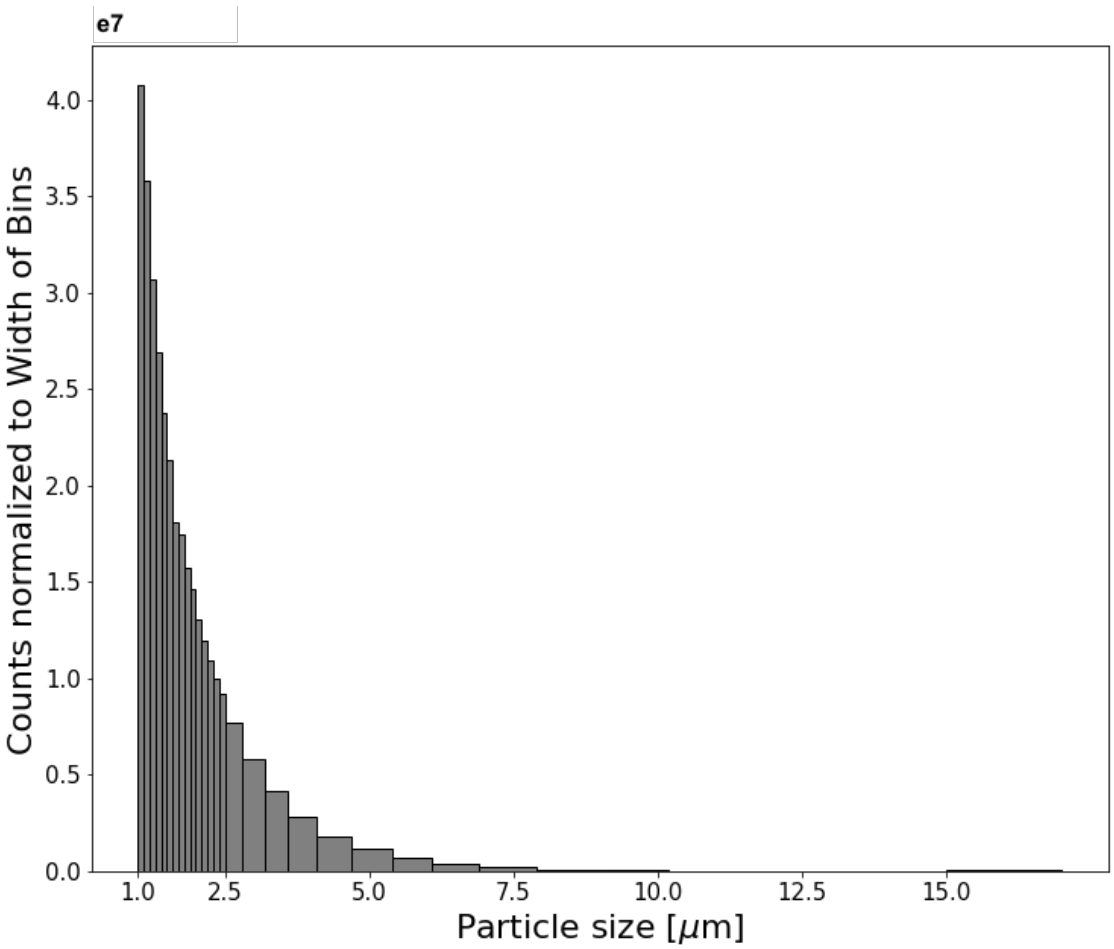

Figure 38: Example: Dust distribution in size-classes after normalisation

4 Results and Discussion

4.1 Dust Timeline

As a result of the ice melting campaign and the subsequent preliminary data-processing we have a large collection of dust-particle counts for a time-span ranging from 39,255 years b2k to 28,842 years b2k. The time-span is situated within the late Pleistocene epoch. A scatter-plot with a marker for the count of particles per ml from every sample shows that 6 distinctive periods with much dust can be identified, as can 5 periods with little dust (see figure (39)). On average the stadials were found to have 5.3 times more dust than the interstadials.

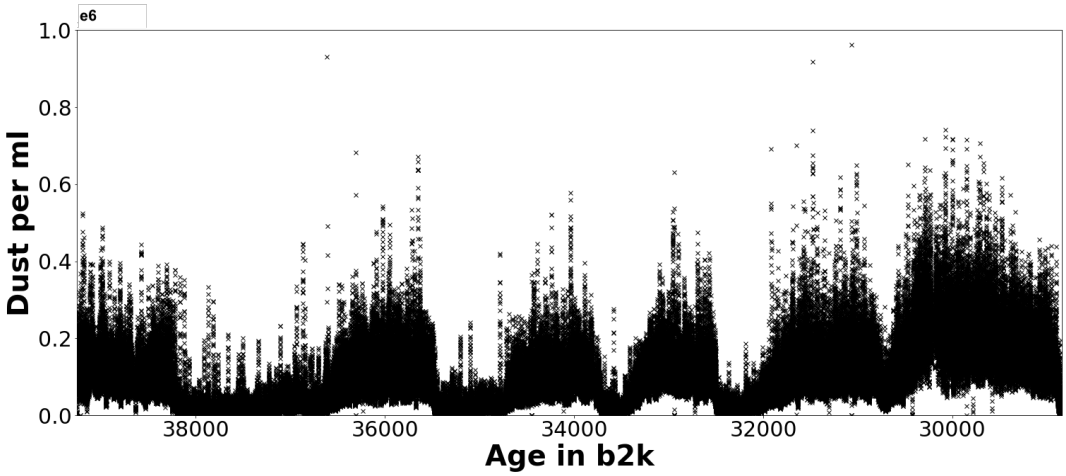

Figure 39: Time-plot of dust per ml in the EGRIP ice core from 1930 meters to 1713 meters deep in the core.

In figure (40) the known DO-events from the timespan in question have been added to the plot. Six of them are the glacial stadials: GS9, GS8, GS7, GS6, GS5.2 and GS5.1, and five of them are the glacial interstadials: GI8, GI7, GI6, GI5.2 and GI5.1 (data taken from "The refined and extended INTIMATE event stratigraphy", - a supplement data-sheet to [15]). As can be seen from the plot, the periods of small and large concentrations of dust coincide well with the defined interstadials and stadials and simple calculations reveal that stadials have up to 8 times more dust than the adjacent interstadials.

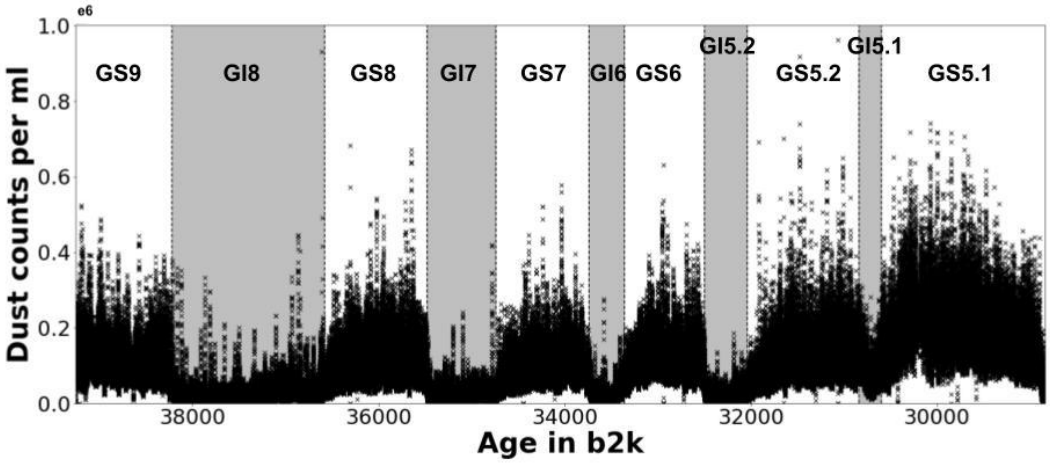

Figure 40: Dust per ml in the EGRIP ice core from 1930 meters to 1713 meters deep in the core with indicated Glacial Stadials (GS) in grey and Glacial Interstadials (GI) in white.

When compared to the course of $\delta^{18}O$ measurements obtained from the NGRIP2 core for the same age period [32] (see figure(41)), the dust profile (figure(40)) exhibits a similar course. The plots reveal, that the periods with lesser dust occurred abruptly and the build-up for the periods with more dust happened gradually just as the $\delta^{18}O$ profile, that reflects an abrupt warming, followed by a gradually cooling down period, lasting several hundred years.

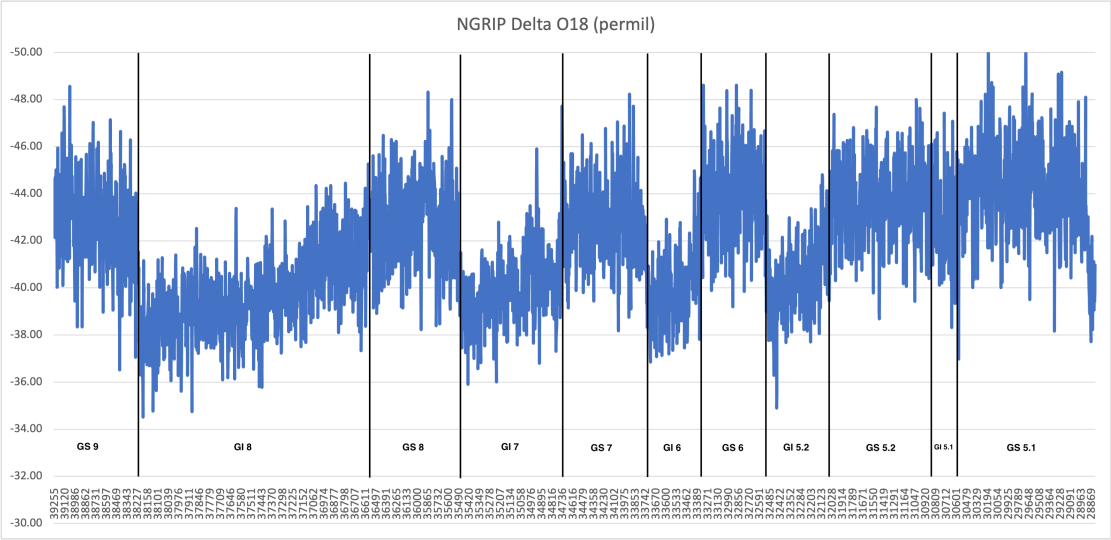

Figure 41: $\delta^{18}O$ measurements over time (GICC05) from NGRIP2 with indicated Glacial Stadials (GS) and Glacial Interstadials (GI)

Based on these observations, it is fair to say, that there is a correlation between dust and climate on a stadial time-scale. Not only the amount of dust correlates to the temperature also the non-sinusoidal variation of these properties seems to have similar pattern. One explanation could be the direct cooling effect of aerial dust as described in section 2.6.

4.2 Comparison to Findings in Ice Cores from earlier Drillings

With only limited access to insoluble dust count records from earlier ice cores drillings, the (soluble) Ca^{2+} parts per billion (ppb) measurements from the North Greenland Ice-Core Project 2 (NGRIP2), the Greenland Ice Core Project (GRIP) and the Greenland Ice Sheet Project 2 (GISP2) were used as a proxy for dust at those sites.

Having a different unit of measurement, the Ca^{2+} values of the NGRIP2, GRIP and GISP2 datasets are multiplied with a factor (≈ 360) in order to re-scale from Ca^{2+} ppb to dust counts/ml. This factor was calculated so that the overall average of NGRIP2, GRIP and GISP2 match the overall average of EGRIP. The resulting values are depicted as "Equivalent of dust counts" in the following figures.

Figure(42) shows a scatter plot of the EGRIP dust counts together with the dust count equivalent of the Ca^{2+} content found in the other ice cores in

the time range from ca. 39,000 years b2k to 29,000 years b2k. The datasets from the three other cores contain the 50-year running average in contradiction to the EGRIP dust data that has a much higher resolution. Visually, it can be seen though, that the Ca^{2+} content of the three older ice cores show the same behaviour as the dust content of the EGRIP ice core analysed in this thesis.

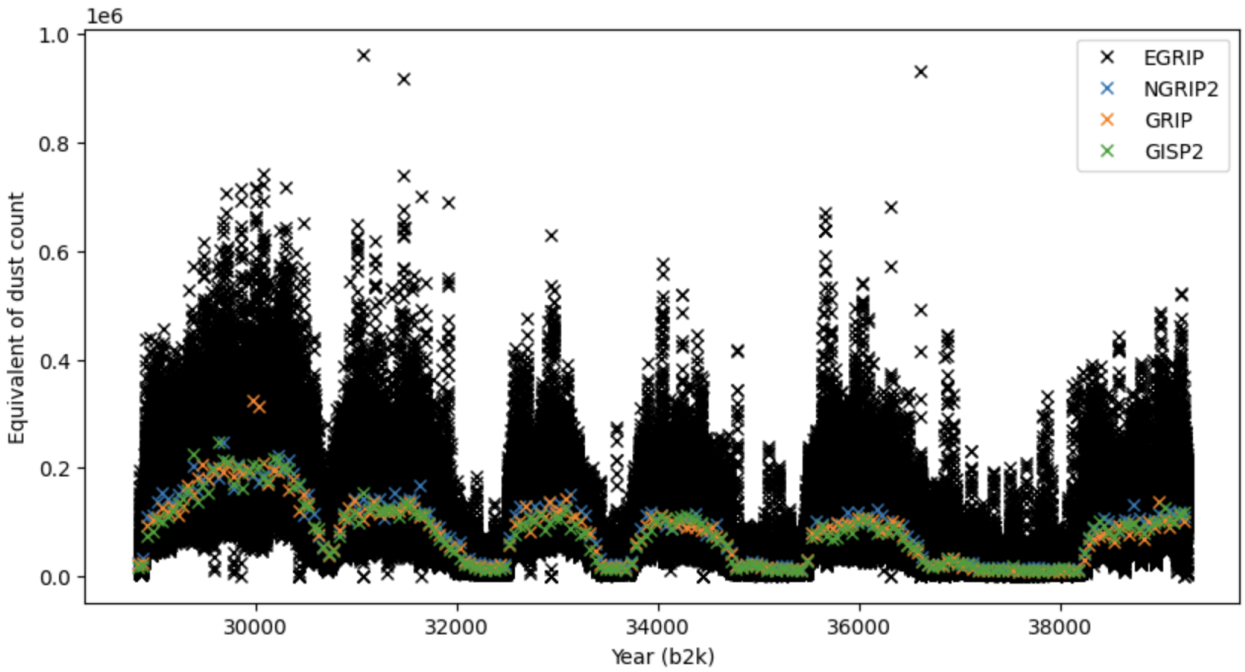

Figure 42: EGRIP dust counts and equivalent 50y-rolling-average counts from NGRIP2, GRIP and GISP2

For a more even-level comparison, a running 50-year average of our dataset is presented in figure (43). The course of our EGRIP dust count is now seen to match the courses of the Ca^{2+} counts fairly well and we may conclude that the profiles are almost proportionally identical and that Ca^{2+} is a good proxy for dust.

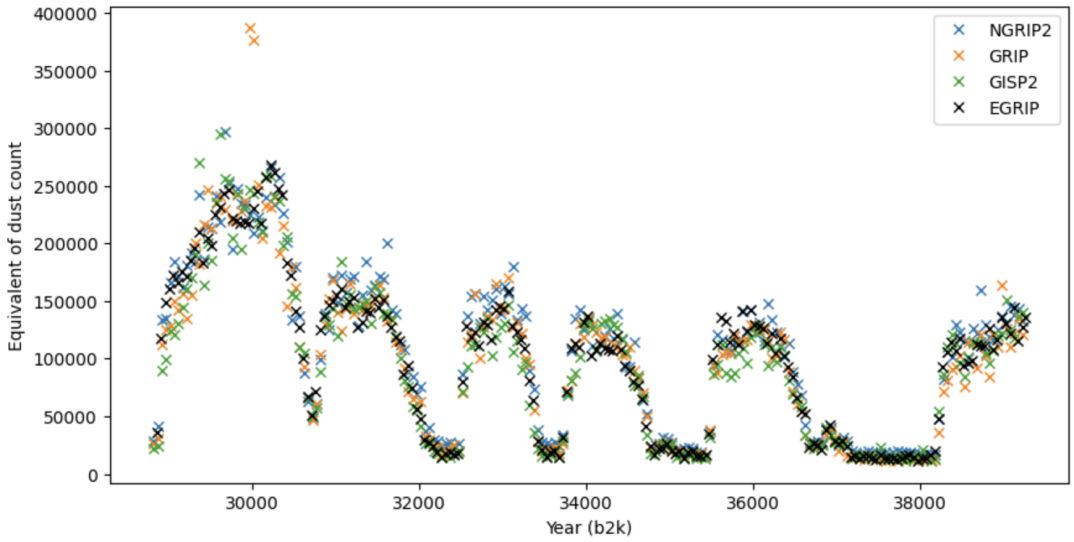

Figure 43: 50y-rolling-average dust counts

Figure(44) presents the deviation of the NGRIP2, GRIP and GISP2 measurements from their common average. For NGRIP2 a generally higher quantity of Ca^{2+} was measured. Apart from that, no spatial or temporal tendencies are seen in the variations from the 50-years averages.

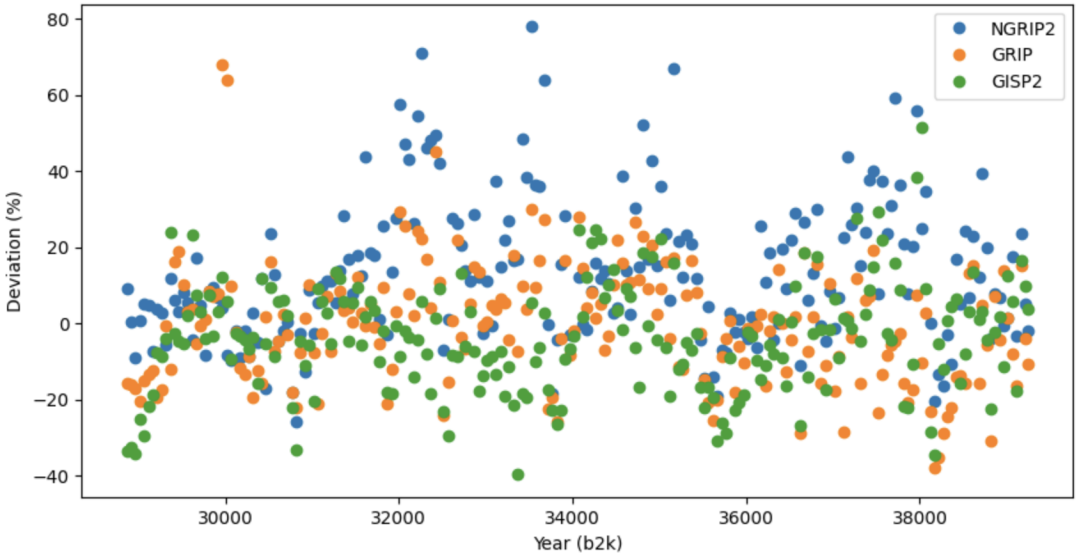

Figure 44: Relative deviation of the 50y-rolling-average Ca^{2+} findings from NGRIP2, GRIP and GISP2 from their common average

4.3 Tephra and Fire Events

Figure (45) lists some key tephra events identified in the Greenland ice cores due to their chemical/mineral structure (see [33] for details).

Greenland ice core tephra layer			Climatic event	Volcanic source	Reference
NGRIP	NEEM	GRIP			
1950.50 m	1689.25 m	-	GI-5	Kverkfjöll	Bourne et al. (2015)
1952.15 m	1690.35 m	-	GS-6	Katla	Bourne et al. (2015)
1954.70 m	-	-	GS-6	Katla	Bourne et al. (2015)
1973.16 m	1702.40 m	-	GI-6	Kverkfjöll	Bourne et al. (2015)
2009.15 m	-	-	GI-7	Hekla	Bourne et al. (2015)
2064.35 m	1755.60 m	2195.45 m	GI-8	Grímsvötn	Bourne et al. (2013, 2015)
2065.65 m	-	-	GI-8	Grímsvötn	Bourne et al. (2013, 2015)
2065.80 m	-	-	GI-8	Grímsvötn	Bourne et al. (2013, 2015)
2066.95 m	1757.10 m	2197.45 m	GI-8	Grímsvötn	Bourne et al. (2013, 2015)
2071.50 m	1759.85 m	2201.50 m	GS-9	Grímsvötn	Bourne et al. (2013, 2015)
2073.15 m	-	-	GS-9	Grímsvötn	Bourne et al. (2013, 2015)
2078.01 m	1764.25 m	2207.00 m	GS-9	Grímsvötn	Bourne et al. (2013, 2015)
2078.37 m	-	-	GS-9	Grímsvötn	Bourne et al. (2013, 2015)
2078.97 m	-	-	GS-9	Grímsvötn	Bourne et al. (2013, 2015)
2079.40 m	-	-	GS-9	Grímsvötn	Bourne et al. (2013, 2015)
2085.80 m	-	-	GS-9	Katla	Bourne et al. (2013, 2015)
2100.65 m	-	-	GS-10	Grímsvötn	Bourne et al. (2013, 2015)
2101.55 m	-	-	GS-10	Grímsvötn	Bourne et al. (2013, 2015)
2103.98 m	1780.20 m	2227.15 m	GS-10	Grímsvötn	Bourne et al. (2013, 2015)

Figure 45: Tephra horizons identified in the Greenland ice core tephra framework [26].

Using the GICC05-EGRIP-1 time scale [23], EGRIP-depth and age are derived from the NGRIP depths of the tephra layers with the results listed in figure (46) and plotted in figure (48).

EGRIP Depth	NGRIP Depth	Age	MCE	DO-Event	Volcano
meters	meters	Years b2k	Years		
1780.95	1950.47	32462	1131	GI-5	Kverkfjöll
1782.70	1952.15	32553	1131	GS-6	Katla
1785.36	1954.70	32724	1131	GS-6	Katla
1805.00	1973.16	33690	1206	GI-6	Kverkfjöll
1844.95	2009.15	35468	1315	GI-7	Hekla
1907.01	2064.35	38040	1440	GI-8	Grímsvötn
1908.48	2065.65	38080	1441	GI-8	Grímsvötn
1908.62	2065.80	38085	1441	GI-8	Grímsvötn
1909.75	2066.95	38121	1441	GI-8	Grímsvötn
1914.59	2071.50	38313	1449	GS-9	Grímsvötn
1916.37	2073.15	38420	1449	GS-9	Grímsvötn
1921.61	2078.01	38735	1449	GS-9	Grímsvötn
1922.00	2078.37	38759	1449	GS-9	Grímsvötn
1922.64	2078.97	38798	1449	GS-9	Grímsvötn
1923.11	2079.40	38825	1449	GS-9	Grímsvötn
1930.01	2085.80	39240	1449	GS-9	Katla
1946.03	2100.65	40203	1449	GS-10	Grímsvötn
1947.00	2101.55	40261	1449	GS-10	Grímsvötn
1949.62	2103.98	40419	1449	GS-10	Grímsvötn

Figure 46: Tephra horizons from fig. (45) related to EGRIP depths and age.

In opposition to the tephra events derived from NGRIP we had no direct records of fire-indicating proxy parameters from Greenland ice cores available for this paper. However, relevant fire dates could be obtained from [28] (see figure 47).

Charcoal identified	MCE
Year (b2k)	Year
22330	130
28290	260
29030	260
31470	360
38250	790
38960	850
39030	890
40000	1000

Figure 47: Calendar data for major central canadian periglacial fires, based on ^{14}C dating of time-stratified charcoal accumulation [28]

In figure (48) the tephra and fire events are marked in a scatter plot of the counts of large particles (15 µm) over time. These events conglomerate in the GS9 stadial, that also exhibits a higher concentration of large particles compared to the more resent stadials. Also the GS5 stadial exhibits a peak in the large particles count. However no tephra of fire event was recorded for GS5, which does not mean, it did not happen. Other (smaller) peaks exist without records of events and visa versa: Events exist without any direct trace of large particles in the ice, which may (especially for the fire events) simply be because there were no wind to carry the particles to the EGRIP site.

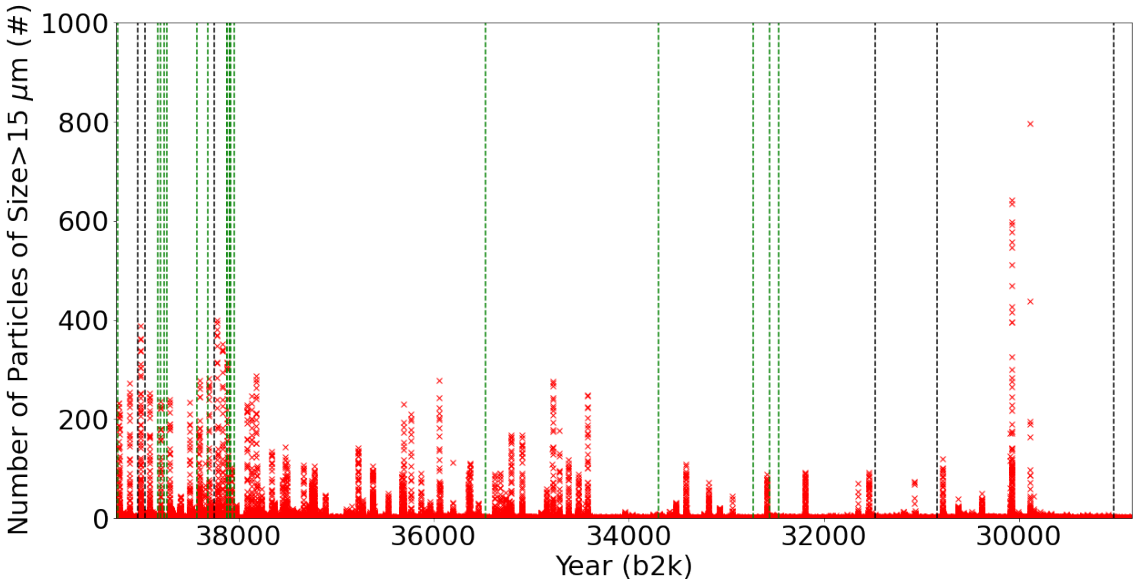

Figure 48: Red points represent the number of particles of a size larger than 15 µm. Times of periglacial fires (see table in fig. 47) are marked with a black line. Times of volcanoes (see table in fig. 46) are marked with a green line.

4.4 Size Distributions of Dust Particles

The total counts of the eleven glacial stadials/interstadials per particle size bin are shown in figure(49). All curves rise in height at a size of 2.5 μm. This is because of a wider bin, as more particles can be counted in a wider bin. The bins become wider with bigger particle sizes because the data file generated by the ABAKUS apparatus is constructed so. Normalising the data with regard to bin widths, gives us the relative distribution of dust sizes for each stadial/interstadial as shown in figure(50). Not surprisingly, the count is high for the smallest particles and decreases with increasing particle size. This corresponds to the spatial behaviour of aerial dust transport as presented in section 2.5 stating that light dust travels further combined with the fact that the dust sources are far away.

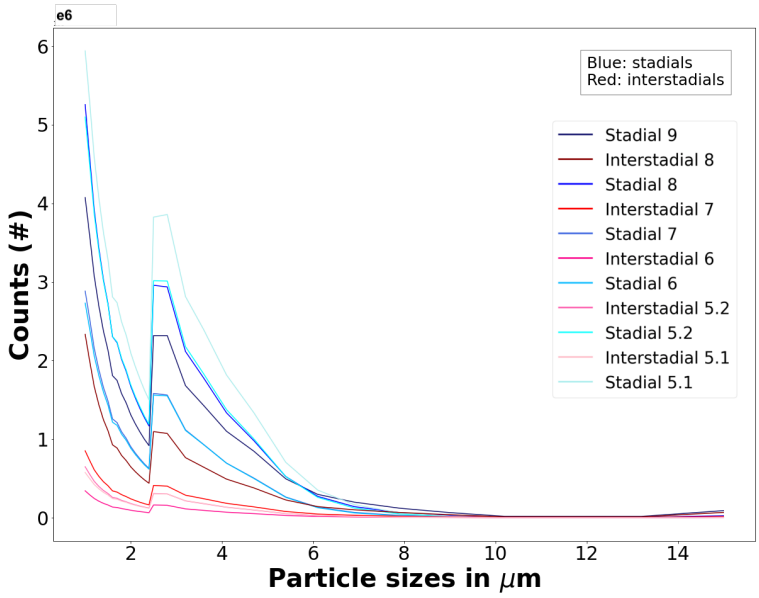

Figure 49: Dust per stadial in millions

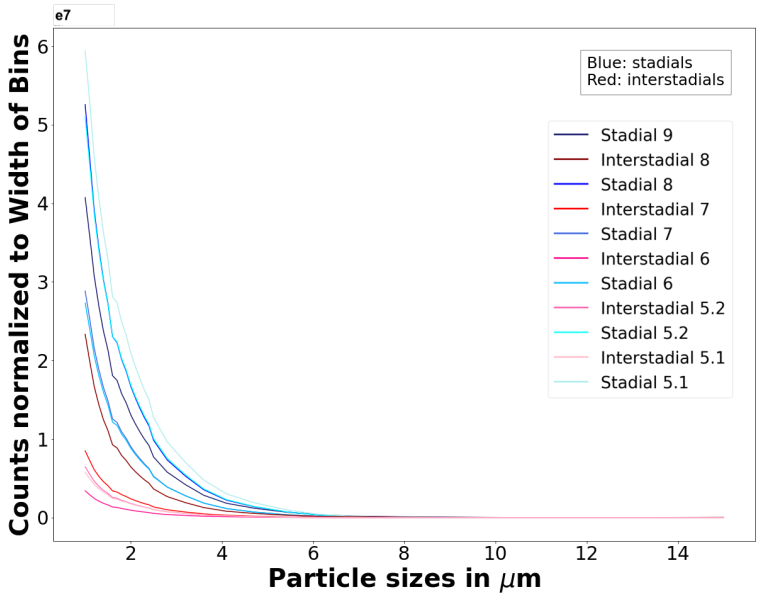

Figure 50: Equivalent dust count per stadial (normalised to a bin-width of 1 µm)

In order to compare the dust deposition of the eleven stadials/interstadials, the dust counts was normalized with regard to the duration of each period. Figure (51) shows the annual dust deposition of each period, with the glacial stadials GS8 and GS5.2 having the highest year-count of small particles. Corresponding to the results of the particle counts presented in section 4.1 we see more dust in the stadials than in the interstadials and there seems to be a significant gap between the dust counts of stadials and interstadials taken as groups (interstadials are reddish and stadial are bluish).

The dust-content is dominated by small particles. The quantity of the larger particles is small in comparison and hard to make out of the plots. Only the absolute counts plotted in figure (49) show more large particles in GS9 than in the other stadials, corresponding to the counts depicted in figure (48).

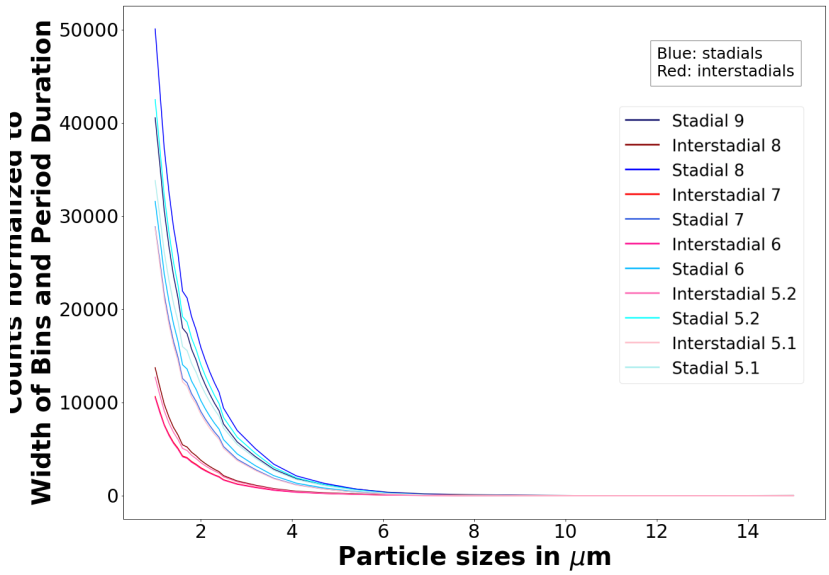

Figure 51: Yearly dust per stadial (normalised regarding bin-width and stadial duration)

Normalizing the yearly dust distributions of figure (51) with regard to the yearly amount of dust in each stadial gives us the relative particle-size distributions shown in figure (52). Even if the amount of dust varies over

the 11 stadials/interstadials with a factor up to 5, the dust mix with regard to particle-size remains more or less constant. This same dust mix in each period indicates similarities in the emission, transport and deposition of dust over Greenland on the large scale.

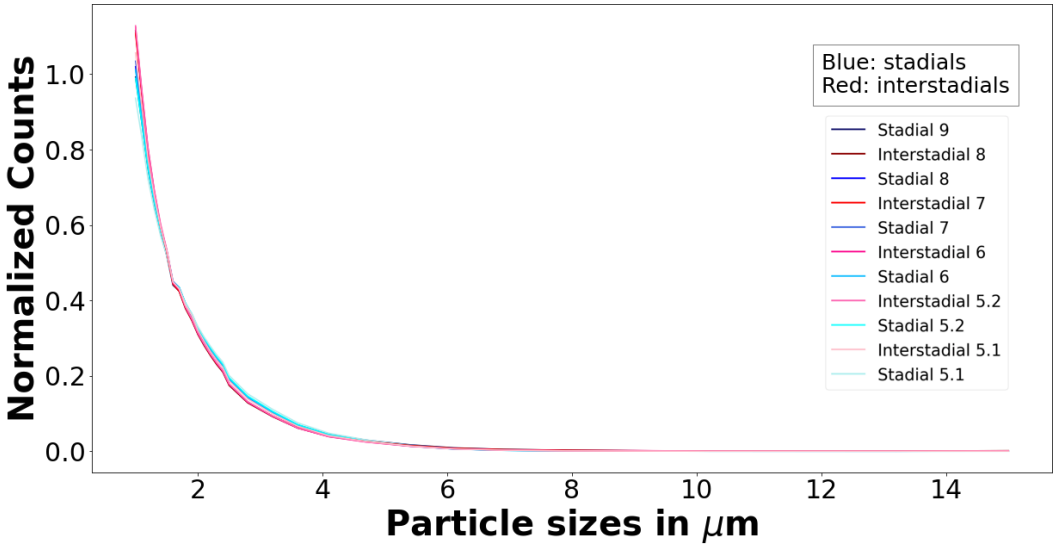

Figure 52: Statistical distribution of particle-size per stadial

4.5 Outlook

A next task could be to further analyse the onset and offset of DO-events by quantifying how fast the dust values fall and how quickly they rise and compare this to the $\delta^{18}O$ measurements. A study of the exact timing of dust change vs $\delta^{18}O$ change might support the theory about dust being a driver for climatic change.

Also, an analysis of the covariance of the dust measurements and $\delta^{18}O$ measurements would be interesting as well as further analysis and comparison of the EGRIP core to multiple other ice cores. This might give deeper insights into the nature of the dust-temperature interlinking.

An analysis of the conductivity measurements of the EGRIP ice core may reveal possible tephra layers in addition to the ones identified by NGRIP. Such observations would allow an EGRIP-specific calender-dating of the volcanic activity and thus a better basis for understanding the role of tephra

for the dust deposition and maybe even for the DO-events. Also, the assessment of further ice-properties from other EGRIP melting campaigns (see fig. (12)) and the comparison with the dust profile might reveal other correlations.

On a longer perspective, hypotheses regarding the dust as driver for climatic change could be refined, statistically tested and used in climate modelling.

5 Conclusion

The presented dust profiles for the time period strongly indicate that there is a correlation between dust and DO-Events on a stadial time-scale. Stadials are relatively dusty, containing on average 5.3 times the dust of interstadials. Not only the amount of dust seems linked to the temperature, but also the non-sinusoidal variation of these properties seems to have similar patterns. One explanation could be the direct cooling effect of aerial dust as described in section 2.6, but it needs further investigations to come to any conclusions. Also, it is impossible to rule out various other hypothesis being the root cause for the DO-events [19, 22], - and for the dust variations as well. With this many climate-influencing phenomenons it is hard to determine which ones are drivers and which ones are results.

The high resolution of our data uncover a fast and large temporal variation in dust count. Applying the 50 year rolling average used in related literature, we find that the EGRIP dust profiles match well with the findings of insoluble dust from NGRIP2, GRIP and GISP2 cores using Ca^{2+} as a proxy.

Dust particle size distributions show a majority of small particles as one would expect, considering the rather long distances from the dust sources and the fact that coarse particles deposit sooner and closer to the source. Despite the variations of dust quantities, the particle-size distribution remained almost the same across stadials and interstadials throughout the observed period. A closer look on the coarse particles ($>$15µm) revealed some peeks where a few of them coincide with tephra or forest fire events, especially in the GS9 stadial. On the other side, there were numerous dust peaks and events, that could not be interlinked. No conclusion on the role of volcanic activity could be made from our results.

Acknowledgements

I owe my thanks to my supervisors Helle and Anders for their kind and valuable guidance and unwavering support. I also owe my thanks to everyone involved in the EGRIP gas campaign for their participation on obtaining the data worked on in this thesis. Finally, I also owe my thanks to everyone else at the Icetunnel and Icecave offices for keeping up the spirit and for entertaining lunch breaks.

References

[1] W. Dansgaard, "The o18-abundance in fresh water," *Geochimica et Cosmochimica Acta*, vol. 6, no. 5, pp. 241–260, 1954.

[2] W. Dansgaard, "Stable isotopes in precipitation," *Tellus*, vol. 16, no. 4, pp. 436–468, 1964.

[3] D. Dahl-Jensen, M. Kirk, I. Koldtoft, T. Popp, and J.P.Steffensen, "Field season 2022 east greenland ice core project (egrip) 2015-2021(2023): Fifth year of egrip deep drilling." https://eastgrip.nbi.ku.dk/documentation/2022/EGRIP2022FieldPlan_1stVersion.pdf, April 2022.

[4] "Master thesis project.docx." Personal coorespondance with Helle Astrid Kjær and Anders Svensson.

[5] S. Mojtabavi, F. Wilhelms, E. Cook, S. M. Davies, G. Sinnl, M. Skov Jensen, D. Dahl-Jensen, A. Svensson, B. M. Vinther, S. Kipfstuhl, G. Jones, N. B. Karlsson, S. H. Faria, V. Gkinis, H. A. Kjær, T. Erhardt, S. M. P. Berben, K. H. Nisancioglu, I. Koldtoft, and S. O. Rasmussen, "A first chronology for the east greenland ice-core project (egrip) over the holocene and last glacial termination," *Climate of the Past*, vol. 16, no. 6, pp. 2359–2380, 2020.

[6] C. M. Nørgaard, "Temperaturen var overraskende varm og svingende, da dinosaurerne gik rundt i sydsverige." https://videnskab.dk/naturvidenskab/temperaturen-var-overraskende-varm-og-svingende-da\-dinosaurerne-gik-rundt-i-sydsverige/, July 2021.

[7] P. Ukkonen, K. Aaris-Sørensen, L. Arppe, P. Clark, L. Daugnora, A. Lister, L. Lõugas, H. Seppä, R. Sommer, A. Stuart, P. Wojtal, and I. Zupiņš, "Woolly mammoth (mammuthus primigenius blum.) and its environment in northern europe during the last glaciation," *Quaternary Science Reviews*, vol. 30, no. 5, pp. 693–712, 2011.

[8] C. Summerhayes, *Earths Evolving Climate: A Geoogical Perspective*. Chichester West Sussex Hoboken NJ: Wiley Blackwell, 2015.

[9] S. on Quarternary Statigraphy, "Subcommission on quarternary statigraphy: Major divisions." http://quaternary.stratigraphy.org/major-divisions/.

[10] U. G. Survey, "How does present glacier extent and sea level compare to the extent of glaciers and global sea level during the last glacial maximum (lgm)?." https://www.usgs.gov/faqs/how-does-present-glacier-extent-and-sea-level-compare\-extent-glaciers-and-global-sea-level.

[11] L. Augustin, C. Barbante, P. R. F. Barnes, J. Marc Barnola, M. Bigler, E. Castellano, O. Cattani, J. Chappellaz, D. Dahl-Jensen, B. Delmonte, G. Dreyfus, G. Durand, S. Falourd, H. Fischer, J. Flückiger, M. E. Hansson, P. Huybrechts, G. Jugie, S. J. Johnsen, J. Jouzel, P. Kaufmann, J. Kipfstuhl, F. Lambert, V. Y. Lipenkov, G. C. Littot, A. Longinelli, R. Lorrain, V. Maggi, V. Masson-Delmotte, H. Miller, R. Mulvaney, J. Oerlemans, H. Oerter, G. Orombelli, F. Parrenin, D. A. Peel, J.-R. Petit, D. Raynaud, C. Ritz, U. Ruth, J. Schwander, U. Siegenthaler, R. Souchez, B. Stauffer, J. Peder Steffensen, B. Stenni, T. F. Stocker, I. E. Tabacco, R. Udisti, R. S. W. van de Wal, M. van den Broeke, J. Weiss, F. Wilhelms, J.-G. Winther, E. W. Wolff, M. Zucchelli, E. community members, and E. community members (participants are listed alphabetically), "Eight glacial cycles from an antarctic ice core," *Nature*, vol. 429, no. 6992, pp. 623–628, 2004.

[12] U. of Calgary, "Glacials and interglacials." https://energyeducation.ca/encyclopedia/Glacial_and_interglacial_periods.

[13] "Geologic time scale: Major eons, eras, periods and epochs." https://www.geologyin.com/2014/12/geologic-time-scale-major-eons-eras.html.

[14] L. NIU, G. LOHMANN, S. HINCK, E. J. GOWAN, and U. KREBS-KANZOW, "The sensitivity of northern hemisphere ice sheets to atmospheric forcing during the last glacial cycle using pmip3 models," *Journal of Glaciology*, vol. 65, no. 252, p. 645–661, 2019.

[15] S. O. Rasmussen, M. Bigler, S. P. Blockley, T. Blunier, S. L. Buchardt, H. B. Clausen, I. Cvijanovic, D. Dahl-Jensen, S. J. Johnsen, H. Fischer, V. Gkinis, M. Guillevic, W. Z. Hoek, J. J. Lowe, J. B. Pedro, T. Popp, I. K. Seierstad, J. P. Steffensen, A. M. Svensson, P. Vallelonga, B. M. Vinther, M. J. Walker, J. J. Wheatley, and M. Winstrup, "A stratigraphic framework for abrupt climatic changes during the last glacial period based on three synchronized greenland ice-core records: refining and extending the intimate event stratigraphy," *Quaternary Sci-*

ence Reviews, vol. 106, pp. 14–28, 2014. Dating, Synthesis, and Interpretation of Palaeoclimatic Records and Model-data Integration: Advances of the INTIMATE project(INTegration of Ice core, Marine and TErrestrial records, COST Action ES0907).

[16] W. Dansgaard, H. B. Clausen, N. Gundestrup, C. U. Hammer, S. F. Johnsen, P. M. Kristinsdottir, and N. Reeh, "A new greenland deep ice core," *Science*, vol. 218, no. 4579, pp. 1273–1277, 1982.

[17] W. Dansgaard, S. Johnsen, H. Clausen, D. Dahl-Jensen, N. Gundestrup, C. Hammer, and H. Oeschger, *North Atlantic Climatic Oscillations Revealed by Deep Greenland Ice Cores*, pp. 288–298. American Geophysical Union (AGU), 1984.

[18] H. Oeschger, J. Beer, U. Siegenthaler, B. Stauffer, W. Dansgaard, and C. Langway, *Late Glacial Climate History from Ice Cores*, pp. 299–306. American Geophysical Union (AGU), 1984.

[19] C. Li and A. Born, "Coupled atmosphere-ice-ocean dynamics in dansgaard-oeschger events," *Quaternary Science Reviews*, vol. 203, pp. 1–20, 2019.

[20] E. Capron, S. O. Rasmussen, T. J. Popp, T. Erhardt, H. Fischer, A. Landais, J. B. Pedro, G. Vettoretti, A. Grinsted, V. Gkinis, B. Vaughn, A. Svensson, B. M. Vinther, and J. W. C. White, "The anatomy of past abrupt warmings recorded in greenland ice," *Nature Communications*, vol. 12, no. 1, p. 2106, 2021.

[21] K. Schepanski, "Transport of mineral dust and its impact on climate," *Geosciences*, vol. 8, no. 5, 2018.

[22] C. Li and A. Born, "Coupled atmosphere-ice-ocean dynamics in dansgaard-oeschger events," *Quaternary Science Reviews*, vol. 203, pp. 1–20, 2019.

[23] "Gicc05-egrip-1-10jun2021.xls time scale for the egrip ice core." Made available from NBI through H. A. Kjær.

[24] A. Svensson, *Ice Cores*, pp. 1–12. Dordrecht: Springer Netherlands, 2013.

[25] N. Mahowald, S. Albani, J. F. Kok, S. Engelstaeder, R. Scanza, D. S. Ward, and M. G. Flanner, "The size distribution of desert dust aerosols and its impact on the earth system," *Aeolian Research*, vol. 15, pp. 53–71, 2014.

[26] A. Bourne, E. Cook, P. Abbott, I. Seierstad, J. Steffensen, A. Svensson, H. Fischer, S. Schüpbach, and S. Davies, "A tephra lattice for greenland and a reconstruction of volcanic events spanning 25–45 ka b2k," *Quaternary Science Reviews*, vol. 118, pp. 122–141, 2015. Synchronising Environmental and Archaeological Records using Volcanic Ash Isochrons.

[27] H. Kjaer, P. Zens, S. Black, K. Lund, A. Svensson, and P. Vallelonga, "Canadian forest fires, icelandic volcanoes and increased local dust observed in six shallow greenland firn cores," *Climate of the Past*, vol. 18, pp. 2211–2230, Oct. 2022.

[28] N. Bélanger, C. Carcaillet, G. Padbury, A. Harvey-Schafer, and K. Rees, "Periglacial fires and trees in a continental setting of central canada, upper pleistocene," *Geobiology*, vol. 12, pp. 109–118, 01 2014.

[29] A. Svensson, K. K. Andersen, M. Bigler, H. B. Clausen, D. Dahl-Jensen, S. M. Davies, S. J. Johnsen, R. Muscheler, F. Parrenin, S. O. Rasmussen, R. Röthlisberger, I. Seierstad, J. P. Steffensen, and B. M. Vinther, "A 60 000 year greenland stratigraphic ice core chronology," *Climate of the Past*, vol. 4, no. 1, pp. 47–57, 2008.

[30] K. K. Andersen, A. Svensson, S. J. Johnsen, S. O. Rasmussen, M. Bigler, R. Röthlisberger, U. Ruth, M.-L. Siggaard-Andersen, J. Peder Steffensen, D. Dahl-Jensen, B. M. Vinther, and H. B. Clausen, "The greenland ice core chronology 2005, 15–42ka. part 1: constructing the time scale," *Quaternary Science Reviews*, vol. 25, no. 23, pp. 3246–3257, 2006. Critical Quaternary Stratigraphy.

[31] A. Svensson, K. K. Andersen, M. Bigler, H. B. Clausen, D. Dahl-Jensen, S. M. Davies, S. J. Johnsen, R. Muscheler, S. O. Rasmussen, R. Röthlisberger, J. Peder Steffensen, and B. Vinther, "The greenland ice core chronology 2005, 15–42ka. part 2: comparison to other records," *Quaternary Science Reviews*, vol. 25, no. 23, pp. 3258–3267, 2006. Critical Quaternary Stratigraphy.

[32] North Greenland Ice Core Project members, K. Andersen, N. Azuma, J.-M. Barnola, M. Bigler, P. Biscaye, N. Caillon, J. Chappellaz, H. Clausen, D. Dahl-Jensen, H. Fischer, J. Flückiger, D. Fritzsche, Y. Fujii, K. Goto-Azuma, K. Grønvold, N. Gundestrup, M. Hansson, C. Huber, C. Hvidberg, S. Johnsen, U. Jonsell, J. Jouzel, S. Kipfstuhl, A. Landais, M. Leuenberger, R. Lorrain, V. Masson-Delmotte,

H. Miller, H. Motoyama, H. Narita, T. Popp, S. Rasmussen, D. Raynaud, R. Röthlisberger, U. Ruth, D. Samyn, J. Schwander, H. Shoji, M. Andersen, J. Steffensen, T. Stocker, A. Sveinbjörnsdóttir, A. Svensson, M. Takata, J.-L. Tison, T. Thorsteinsson, O. Watanabe, F. Wilhelms, and J. White, "High-resolution record of northern hemisphere climate extending into the last interglacial period," *Nature*, vol. 431, pp. 147–151, 2004. Paper id:: doi:10.1038/nature02805.

[33] S. M. Berben, T. M. Dokken, P. M. Abbott, E. Cook, H. Sadatzki, M. H. Simon, and E. Jansen, "Independent tephrochronological evidence for rapid and synchronous oceanic and atmospheric temperature rises over the greenland stadial-interstadial transitions between ca. 32 and 40 ka b2k," *Quaternary Science Reviews*, vol. 236, p. 106277, 2020.

[34] S. O. Rasmussen, M. Bigler, S. P. Blockley, T. Blunier, S. L. Buchardt, H. B. Clausen, I. Cvijanovic, D. Dahl-Jensen, S. J. Johnsen, H. Fischer, V. Gkinis, M. Guillevic, W. Z. Hoek, J. J. Lowe, J. B. Pedro, T. Popp, I. K. Seierstad, J. P. Steffensen, A. M. Svensson, P. Vallelonga, B. M. Vinther, M. J. Walker, J. J. Wheatley, and M. Winstrup, "A stratigraphic framework for abrupt climatic changes during the last glacial period based on three synchronized greenland ice-core records: refining and extending the intimate event stratigraphy," *Quaternary Science Reviews*, vol. 106, pp. 14–28, 2014. Dating, Synthesis, and Interpretation of Palaeoclimatic Records and Model-data Integration: Advances of the INTIMATE project(INTegration of Ice core, Marine and TErrestrial records, COST Action ES0907).

A Appendix

The programming code used for this thesis can be found under the following link:
https://github.com/cecilieboy/Dust

Event	Age (b2k)
Start of GS-5.1	30,600
Start of GI-5.1	30,840
Start of GS-5.2	32,040
Start of GI-5.2	32,500
Start of GS-6	33,360
Start of GI-6	33,740
Start of GS-7	34,740
Start of GI-7	35,480
Start of GS-8	36,580
Start of GI-8	38,220
Start of GS-9	39,900

Table 1: Starting ages of stadials and interstadials (reproduced from: [34]).